



January 2012

A Geophysical Investigation Of The Northeastern Rim Of The St. Martin Impact Structure, Manitoba, Canada.

Vladimir B. Zivkovic

Follow this and additional works at: <https://commons.und.edu/theses>

Recommended Citation

Zivkovic, Vladimir B., "A Geophysical Investigation Of The Northeastern Rim Of The St. Martin Impact Structure, Manitoba, Canada." (2012). *Theses and Dissertations*. 1225.
<https://commons.und.edu/theses/1225>

This Dissertation is brought to you for free and open access by the Theses, Dissertations, and Senior Projects at UND Scholarly Commons. It has been accepted for inclusion in Theses and Dissertations by an authorized administrator of UND Scholarly Commons. For more information, please contact zeinebyousif@library.und.edu.

A GEOPHYSICAL INVESTIGATION OF THE NORTHEASTERN RIM OF THE ST.
MARTIN IMPACT STRUCTURE, MANITOBA, CANADA.

by

Vladimir B. Zivkovic

Bachelors of Science, Temple University, Philadelphia, PA, December, 2000

Master of Science, University of Memphis, Memphis, TN, December, 2006

A Dissertation

Submitted to the Graduate Faculty

of the

University of North Dakota

in partial fulfillment of the requirements

for the degree of

Doctor of Philosophy

Grand Forks, North Dakota

May
2012

This dissertation, submitted by Vladimir B. Zivkovic in partial fulfillment of the requirements for the degree of Doctor of Philosophy from the University of North Dakota has been read by the Faculty Advisory Committee under whom the work has been done and is hereby approved.

William D. Gosnold

Chairperson

Dexter Perkins

Mike Gaffey

Zheng-Wen Zeng

Marcellin Zahui

This dissertation meets the standards for appearance, conforms to the style and format requirements of the Graduate School of the University of North Dakota, and is hereby approved.

Wayne Swisher

Dean of the Graduate School

May 3, 2012

Date

PERMISSION

Title A Geophysical Investigation of the Northeastern Rim of the St. Martin
Impact Structure, Manitoba, Canada.

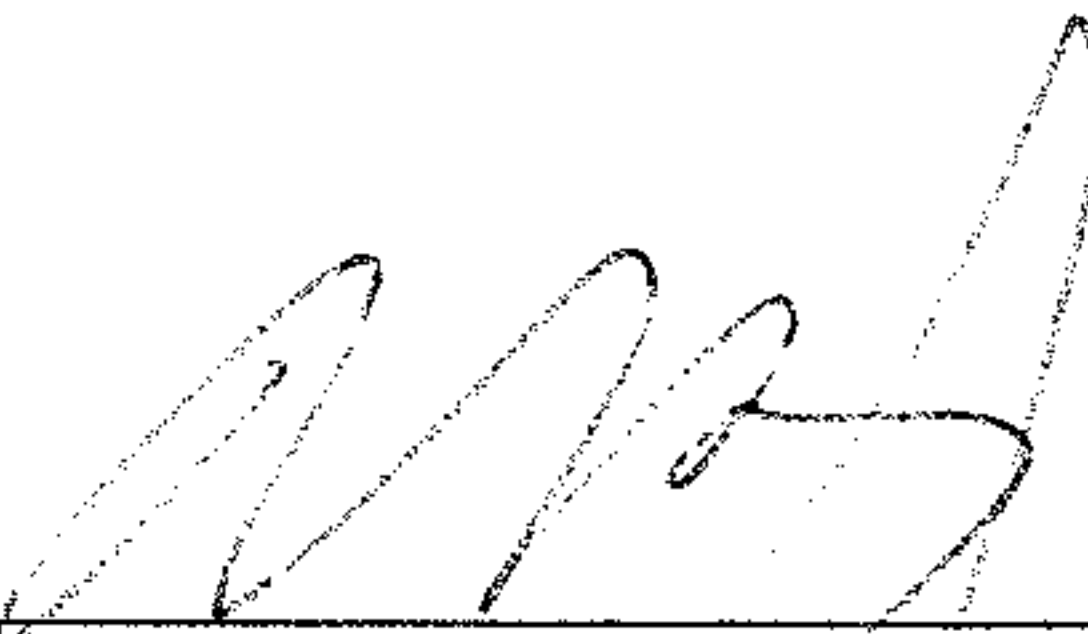
Department Geology and Geological Engineering

Degree Doctor of Philosophy

In presenting this dissertation in partial fulfillment of the requirements for a graduate degree from the University of North Dakota, I agree that the library of this University shall make it freely available for inspection. I further agree that permission for extensive copying for scholarly purposes may be granted by the professor who supervised my dissertation work or, in his absence, by the chairperson of the department or the dean of the Graduate School. It is understood that any copying or publication or other use of this dissertation or part thereof for financial gain shall not be allowed without my written permission. It is also understood that due recognition shall be given to me and to the University of North Dakota in any scholarly use which may be made of any material in my dissertation.

Signature

Date



4/30/12

TABLE OF CONTENTS

LIST OF FIGURES.....	vi
LIST OF TABLES.....	viii
ACKNOWLEDGMENTS.....	ix
ABSTRACT.....	x
CHAPTER	
I. INTRODUCTION.....	1
Hypothesis.....	1
Geologic Background.....	1
Age of Impact.....	3
Types of Impact Craters.....	4
Lake Saint Martin Morphology.....	5
Structure Lithology.....	6
II. THEORY AND APPLICATIONS OF METHODS USED.....	9
Gravitational Acceleration.....	9
Magnetism.....	10
Observed vs. Calculated Values.....	10
Gravity and Magnetic Surveys of Impact Craters.....	11
Reflection Seismology.....	14

III.	PREVIOUS GRAVITY WORK.....	16
	Gravity Results.....	16
IV.	MAGNETICS.....	25
	Data Acquisition.....	25
	Data Reduction.....	26
	Attenuation of Error.....	27
V.	SEISMIC REFLECTION PROFILING.....	32
	Data Acquisition.....	32
	Energy Source.....	33
	Technique.....	33
	Normal Move Out.....	34
	Data Reduction.....	34
VI.	RESULTS.....	36
	Gravity.....	36
	Magnetic.....	38
	Seismic Reflection Profiling.....	42
VII.	DISCUSSION.....	46
	REFERENCES CITED.....	48

LIST OF FIGURES

Figure	Page
1. Location of the St. Martin Impact structure depicting selected core hole locations and structure boundary.....	2
2. Stratigraphic column of the Lake St. Martin area.....	3
3. Figure depicting the structural differences between a simple crater and a complex crater.....	4
4. Location of Silurian-Ordovician surface samples used to determine slope of the structure.....	6
5. Geologic Cross Section of the St. Martin impact structure based on magnetic data points with selected core hole locations	8
6. Geologic cross section and typical magnetic and gravity profile of a hypothetical simple crater.....	12
7. Geologic cross section and typical magnetic and gravity profile of a hypothetical complex crater.....	12
8. Geologic cross section and typical magnetic and gravity profile of a hypothetical simple crater with accompanying lithology.....	13
9. Geologic cross section and typical magnetic and gravity profile of a hypothetical complex crater with accompanying lithology.....	14
10. Diagram indicating symbols used for reflection travel time curves.....	15
11. Gravity survey locations.....	17
12. First order polynomial trend surface of the Bouguer anomaly with the structures outline superimposed.....	17
13. Second order polynomial trend surface of the Bouguer anomaly.....	18
14. Third order polynomial trend surface of the Bouguer anomaly.....	18
15. Lake St. Martin Bouguer gravity anomaly map with gravity station locations.....	20

16. A 3D wireframe of the Bouguer gravity anomaly map revealing the southwesterly slope of the impact structure.....	21
17. Lake St. Martin 1st order residual gravity.....	22
18. Lake St. Martin 2nd order residual gravity.....	23
19. Lake St. Martin 3rd order residual gravity	24
20. Magnetic Data Points	26
21. Daily diurnal variation during the magnetic survey	31
22. Ariel view of the location of the seismic reflection line.....	32
23. The Ballistic Ordinance Seismic Source, (BOSS).....	33
24. Ray paths of reflections belonging to the common depth point (CDP) which is located below the shot-geophone common midpoint, O.....	34
25. Multiple seismic shotpoints from the seismic line prior to data processing.....	35
26. Seismic line gravity profile.....	38
27. Remnant magnetic field strength and data points with superimposed crater boundary.....	40
28. Magnetic profile of seismic line with depth to anomaly.....	40
29. Combined geologic profile with accompanying gravity and magnetic data	31
30. Seismic reflection image of Big Rock depicting associated features.....	43
31. $x^2 - t^2$ values of three shot locations used to determine velocity and thickness.....	43
32. Beginning shot gather with first breaks.....	44
33. Middle shot gather with first breaks.....	44
34. Last shot gather with first breaks.....	45

LIST OF TABLES

Table	Page
1. Magnetic data point locations with anomaly values.....	28
2. Data processing flow.....	35
3. Selected gravity stations used in the gravity profile of Big Rock.....	37

ACKNOWLEDGMENTS

First I would like to thank the University of North Dakota and the Graduate School for accepting me into their prestigious institution. Second, I would like to extend my warmest gratitude to all of my committee members for their gracious support through this arduous journey: William Gosnold, Dexter Perkins, Zheng-Wen Zeng, Mike Gaffey, and Marcellin Zahui. Third, to my wife Monique and children: Cameron, Clayton, and Kierra who all had to suffer in -50 degree winters (wind chill included) to allow me to pursue my goal. Fourth, my father who came to America with nothing and inspired me to achieve more. And last but not least, to George Takei, who on the campus of Temple University on a brisk autumn day, told me to ‘Reach for the Highest Star’...and I did!

ABSTRACT

The St. Martin impact structure is a 40 Km diameter structure located in Manitoba, Canada lies in featureless, glaciated terrain lacking any surface expression of an impact structure. The age of the structure has been re-determined to range between 224.3 Ma to 241.4 Ma which nullified a previous hypothesis suggesting this impact was part of a multiple impact event. Within the proposed structural boundary two outcrops of Archean granite are present. The first outcrop is located in what has been identified as the central peak of the impact structure. The second outcrop lies along the northeastern boundary and is known locally as Big Rock. The purpose of this investigation was to determine the relationship of Big Rock, if any, to the impact event and to constrain a more accurate diameter of the structure.

To accomplish this I conducted two geophysical surveys and used selected data from a previous survey. The two methods I conducted were: a magnetic survey and seismic reflection profiling. Selected data from a previous gravity survey was used to supplement survey results. The magnetic survey was conducted using the total field G-856 Memory-Mag proton precession magnetometer which measures local or regional field strength. The seismic reflection survey was conducted using three Geometrics Geode exploration seismographs. Due to the complexity of seismic data processing I retained an outside seismic data processing company. Previous gravity anomaly data were acquired using a LaCoste and Romberg Model G gravimeter.

The results of this geophysical investigation reveal a shallowing of granitic basement rock with exposure near Big Rock. However, a suggested listric fault near Big

Rock was not identified via seismic reflection profiling, but was suggested by both the gravity and magnetic surveys. Listric faults that are genetically related to impact structures are also indicative of the structure's outer boundary and therefore can confirm that the St. Martin impact structure is indeed 40 Km in diameter.

CHAPTER I

INTRODUCTION

Hypothesis

Impacts between Earth and large interplanetary objects result in violent collisions. One aspect of these collisions is the propagation of shockwaves throughout the impacted body. These impacts generate instantaneous stresses in the GPa range, (Pierazzo and Melosh, 2000b), and result in features associated with impacts. Located in Manitoba, Canada, the Saint Martin impact structure features two Archaean granite outcrops positioned 150 meters above other outcrops of the same age. The first is a crystalline melt sheet near the structures center and the second outcrop is larger and is on the northeast rim of the structure. The hypothesis for this investigation is that the local feature known as Big Rock is uplifted basement rock that resulted from the impact event.

Geologic Background

The St. Martin impact structure (Fig. 1) lies in the Interlake region of Manitoba, Canada at 51.778978 / -98.512679 in featureless glaciated terrain that shows no surface expression suggesting an impact crater. The structure lies on the eastern margin of Paleozoic sedimentary rocks that overlie the Precambrian craton in southern Manitoba. Figure 1 outlines the lateral extent of the impact structure (inner circle) and the extent of disturbed basement rock outside the structure (outer circle), (Pilkington and Grieve, 1992).

Approximately 200 meters of Ordovician-Silurian sedimentary rocks cover the craton in the region and parts of the crater contain Jurassic age sedimentary rocks, Fig. 2, (McCabe and Bannatyne, 1970). Two outcrops of granite currently stand at least 150 meters above the planar surface of the Precambrian basement. The first occurs near the crater center and another 9 kilometers east of the center of the structure (McCabe and Bannatyne, 1970). A 316 meter core hole near the central peak penetrated brecciated granitic rocks its entire length. This core hole showed that the central peak rises at least to the level of the crater rim. Several core holes in the crater show the existence of a 70 meter thick melt sheet east of the central uplift (McCabe and Bannatyne, 1970).

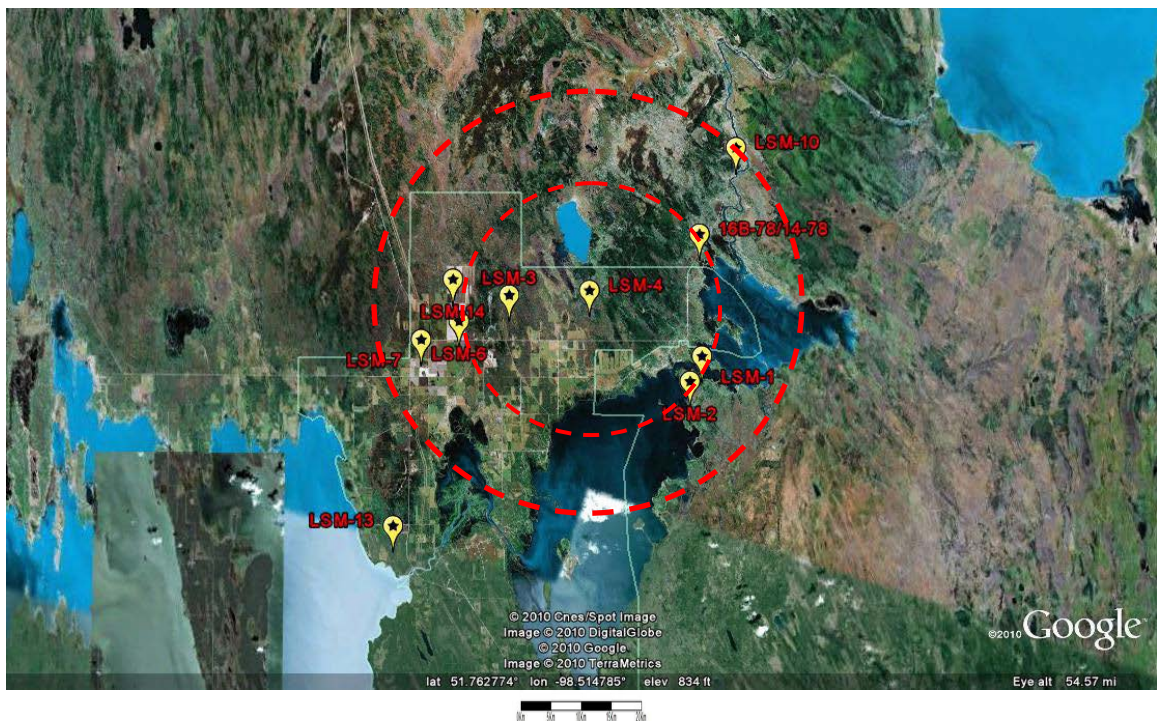


Fig. 1. Location of the St. Martin Impact structure depicting selected core hole locations and structure boundary. Modified from Bannatyne & McCabe, 1984.

Era	Period	Rock Unit		
		Formation	Member	
Cenozoic	Quaternary			
Mesozoic	Jurassic	Amaramth	Evaporite	
			Red Bed	
Paleozoic	Permian	St. Martin Series		
	Devonian		Souris River	
			Dawson Bay	
			Elm Point/Prairie Evaporite	
			Ashern	
	Silurian		Upper Lake	
			Present Erosional Surface	
			Lower Lake	
	Ordovician		Stonewall	
			Stony Mountain	Gunton
				Gunn (Stony Mountain Shale)
			Red River	Fort Garry
Selkirk				
Cat Head				
Winnipeg	Dog Head			
	Precambrian			

Fig. 2. Stratigraphic column of the Lake St. Martin area, modified from McCabe and Bannatyne, 1970. Erosional events are represented by a dashed line.

Age of Impact

Using (U-Th)/He analysis of zircon and apatite samples collected from melt sheet samples 9 Km northeast of the central peak, Wartho et al. (2009) determined the age of the impact as 235.2±6.2 Ma (zircon) and 231.5±7.2 Ma (apatite) placing it in the Middle

to Late Triassic. This age nullifies the hypothesis proposed by Spray (1998) that the St. Martin impact structure is one of five impact events that occurred simultaneously at about 213 Ma.

Types of Impact Craters

Two basic crater structures exist, simple and complex, each produced because of intrinsic variables related to the impacting bolide and target. Bolide variables considered are size, density, composition, angle of impact, and velocity. Target variables to consider are planetary gravity, atmospheric density, target composition, and strength of the target material (Melosh, 1989). A bowl shaped depression and structurally upraised fractured rims characterize simple structures. The complex crater's structure contains a central peak feature, ring structures, and outer fracture zones, Fig. 3.

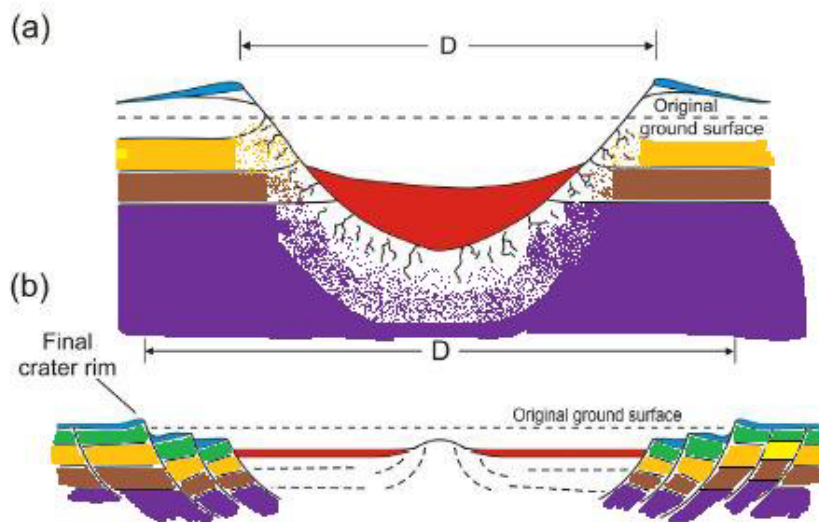


Fig. 3. Figure depicting the structural differences between a simple crater and a complex crater. Modified from NASA, http://rst.gsfc.nasa.gov/Sect18/Sect18_4.html

Lake Saint Martin Morphology

The St. Martin impact structure is a complex crater and is approximately 40 kilometers in diameter, exhibits a central peak, outer fracture zones and contains a 70 meter thick melt sheet to the east (McCabe and Bannatyne, 1970). Glaciation has eroded the Interlake region giving the impact structure no recognizable surface expression.

McCabe and Bannatyne (1970) collected surface samples from exposed outcrops of Paleozoic strata and calculated the structure having a slope of approximately 1.89 meters per kilometer to the west-southwest, Fig. 4. A comparison with an area to the southwest shows that approximately 60 percent of this slope occurred during the post middle Jurassic. This equates to 0.95 meters per kilometer over the crater structure since the Permian or 30.5 meters of post crater tilting. This tilting could be the reason as to the lack of an exposed outcrop toward the western crater rim (McCabe and Bannatyne, 1970).

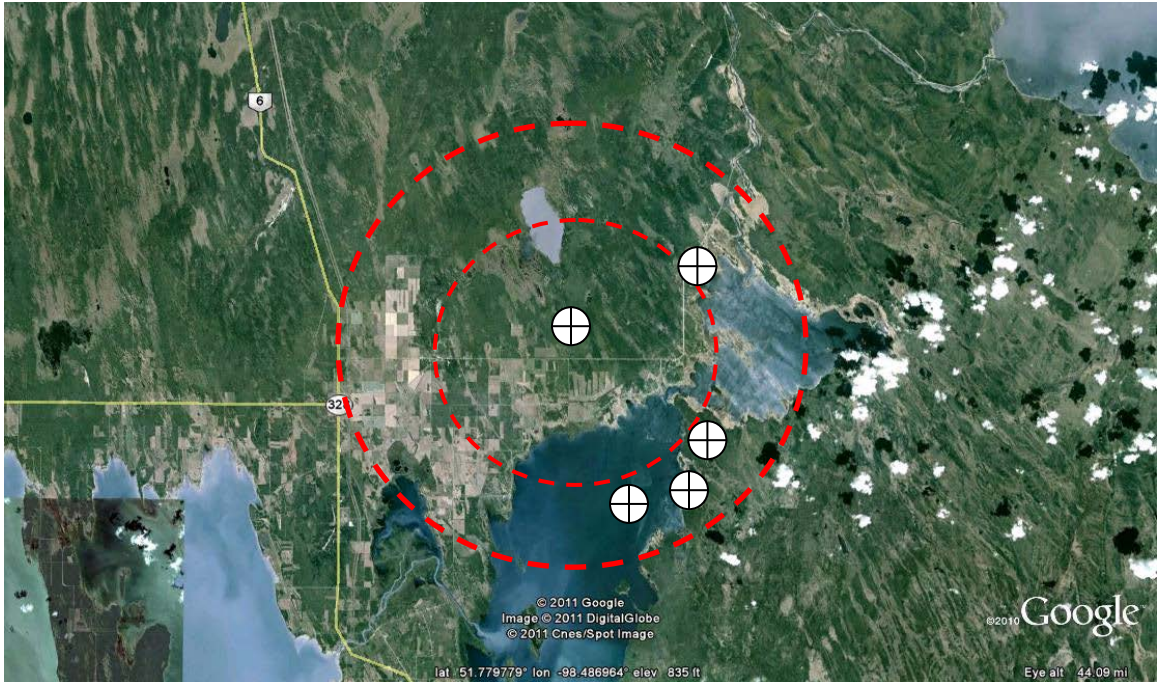


Fig. 4. Location of Silurian-Ordovician surface samples used to determine slope of the structure. Modified from McCabe and Bannatyne, 1970.

Structure Lithology

Figure 5 shows an approximate cross section of the structure and surrounding area with associated lithology as determined from core-hole data. The base of the crater is Superior Province Precambrian granite and gneiss basement rock. Extensive areas of shocked metamorphic features occur within the structure and a 70 meter thick melt-sheet lies on the east side of the crater (McCabe and Bannatyne, 1970). Overlying the Precambrian granite within the structure is: the St. Martin Series composed of Syn-formational Permian igneous polymictic breccia and carbonate breccia. Overlying the St. Martin Series are the Post-formational Jurassic evaporates and Redbeds.

Outside of the impact structure overlying the Precambrian granite is: Ordovician Winnipeg, Red River, Stony Mountain, Stonewall formations. The Interlake Group of Silurian carbonates and shale follows these formations.

McCabe and Bannatyne (1970) assign the St. Martin Series carbonate breccias to the Paleozoic sequences due to extensive faulting, brecciation, mixing and uncertainty as to age. Saint Martin Series breccias have a high concentration of calcium carbonate, dense, microcrystalline and light grey-buff in color. Argillaceous limestone and calcareous shale's are common near the bottom of the core and they exhibit no shock metamorphic features.

Three borings in the St. Martin impact structure produced polymict breccias. These breccias are primarily composed of granite fragments and are light purplish-grey in color. The granitic clasts and other igneous clasts present are generally sub-rounded to well rounded in shape. The St. Martin series has varied thickness but ranges from 3.35 meters to 265 meters.

McCabe and Bannatyne (1970) have recognized aphanitic igneous rocks in only two locations within the crater fill that they identify as trachyandesites. McCabe and Bannatyne (1970) note that the term trachyandesite is based on chemical and petrographic analysis and they imply no origination with the use of this term. Unit thickness ranges from 10.6 meters in boring LSM-3 to 65.2 meters in boring LSM-1. The Isotope and Nuclear Geology Section of the Geological Survey of Canada conducted age determinations on two samples via K-Ar whole rock analyses. Results on the samples showed an age of 250 ± 25 Ma. and 200 ± 25 Ma. respectively, but were revised in 2009 by Wartho to 235.2 ± 6.2 Ma (zircon) and 231.5 ± 7.2 Ma (apatite).

Overlying the trachyandesites are the Red Bed and evaporite units. The Red Beds are approximately 40 meters thick and are composed of reddish brown argillaceous dolomitic siltstones and sandstones. Overlying the Red Beds are 42 meters of the evaporite unit composed of gypsum and anhydrite. McCabe and Bannatyne (1970) assume this sequence to only be present within the crater. Stott (1955) and Bannatyne (1959) have assumed that these units are of similar composition to the Amaranth Formation in southwestern Manitoba that is of Jurassic or Jura-Triassic in age.

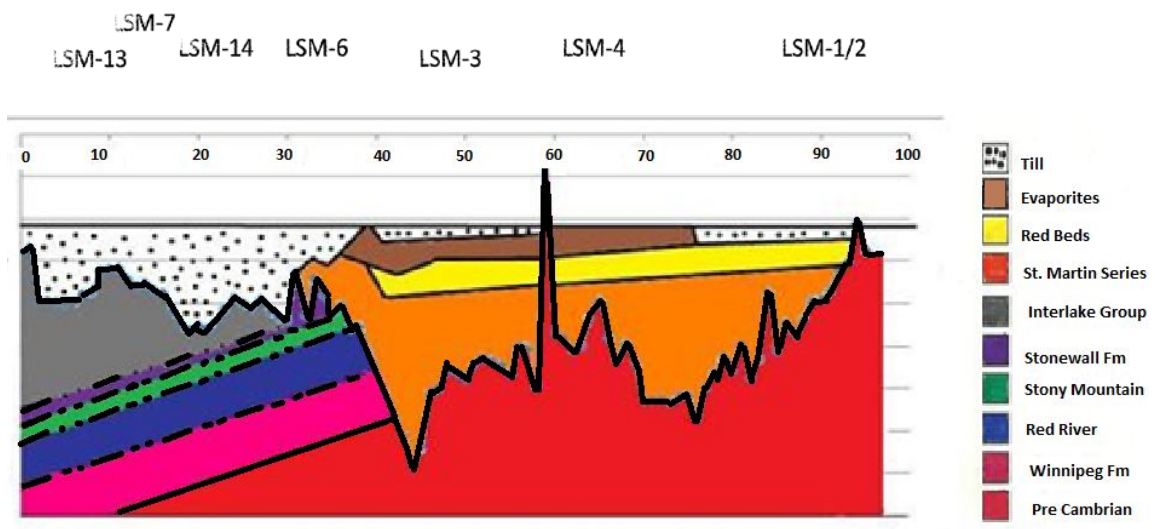


Fig. 5. Geologic Cross Section of the St. Martin impact structure based on magnetic data points with selected core hole locations. Modified from Kohn, B., Osadetz, K., & Bezys, R., 1995.

CHAPTER II
THEORY AND APPLICATIONS OF METHODS USED
Gravitational Acceleration

If Earth were a homogeneously, non-rotating, perfect sphere, the gravitational acceleration (g), would not vary over the surface. Since this is not true and g varies, these measurable variations in g have become invaluable at investigating what lies below the surface. Defining the gravitational acceleration of Newton's second law of motion in terms of g , the equation becomes:

$$g = F/m$$

where F is the force of attraction between two mass points, m is the mass of the object. One of two conventional designations may represent units for gravity: the S.I unit (m/s^2), and the centimeter gram second, c.g.s., system (cm/s^2). As used in geophysics the c.g.s. system is referred to as the gal, in honor of Galileo. One-tenth of a milligal (0.1 mGal) is called a gravity unit, g.u., and is used in exploration work.

Variations in g may be the result of both visible and non-visible features such as mountain ranges, canyons, buried faults, or lateral lithologic changes. The primary factors controlling density are mineral assemblages, fractures, porosity, and saturation. In this study I have investigated a 3 km transect along the suggested northeastern rim of the impact structure utilizing relevant, previously collected gravity data points.

Magnetism

The Earth's magnetic field is a vector quantity and is composed of seven vectors. These vectors are: F, the total intensity of the magnetic field, H, the horizontal component, Z, the vertical component, X, the north component, Y, the east component, D, the magnetic declination and I, magnetic inclination. Remnant magnetization (J_r) is also of primary interest in this study and occurs when host rock, usually igneous, sufficiently melts allowing magnetically susceptible minerals to align themselves parallel to the current magnetic field. This effect is referred to as thermoremanent magnetization (TRM). The presence of a melt sheet at the site indicates that the Curie temperature for magnetite (580°C for magnetite) was achieved. In this study I took into consideration remnant magnetization and measured the F component which is defined by the equation:

$$F = \sqrt{X^2 + Y^2 + Z^2}$$

Observed vs. Calculated Values

In Figures 6 through 9 I have constructed hypothetical impact crater models. These models only contain 'observed' data and no calculated or theoretical values. In terms of gravity the theoretical gravity value would be the value if Earth were a non-rotating, homogenous perfect sphere. The theoretical value does not change. The observed gravity value is the value recorded at a specific location and may change after a geologic event. In terms of the geomagnetic field the magnetic moment would point towards Earth's geographical south and slightly inclined to Earth's geographical axis (Parasnis, D. S., 1997). Again, the theoretical value does not change whereas the observed value may in response to a geologic event.

Gravity and Magnetic Surveys of Impact Craters

Of the greater than 170 known impacts few offer a physical manifestation reminiscent of their true origin. Two notable exceptions are Barringer Crater, a simple crater, located near Flagstaff, Arizona and Upheaval Dome, a complex crater, in Utah. Both gravity and magnetic geophysical methods have discovered a majority of the known impact sites usually by airborne methods.

Magnetic anomaly signal strength primarily depends on the concentration of magnetic minerals present and source depth; with a deeper source resulting in a weaker signal. Since igneous rock usually contains some magnetic minerals the magnetic method generally produces a good profile of the bedrock while ignoring any sedimentary cover. Gravity anomalies are referred to as either positive or negative when referenced to the geoid. A positive anomaly is denser while conversely a negative anomaly is less dense. Factors contributing to the gravity anomaly are type of rock or deposits, fracturing or jointing, and void space. Gravity data may also be used to generate a profile however multiple factors must be considered before doing so. In the following chapters considerations to both magnetic and gravity data will be discussed.

In Figures 6 and 7 I have constructed both a simple, and complex crater geologic cross section with magnetic and gravity profiles without any subsequent fill. Figures 8 and 9 illustrate a hypothetical structure with accompanying lithology. Filling both structures I have used lithology that might accompany the structures such as suevite, shale, dolomite, limestone and a till or other unconsolidated cover.

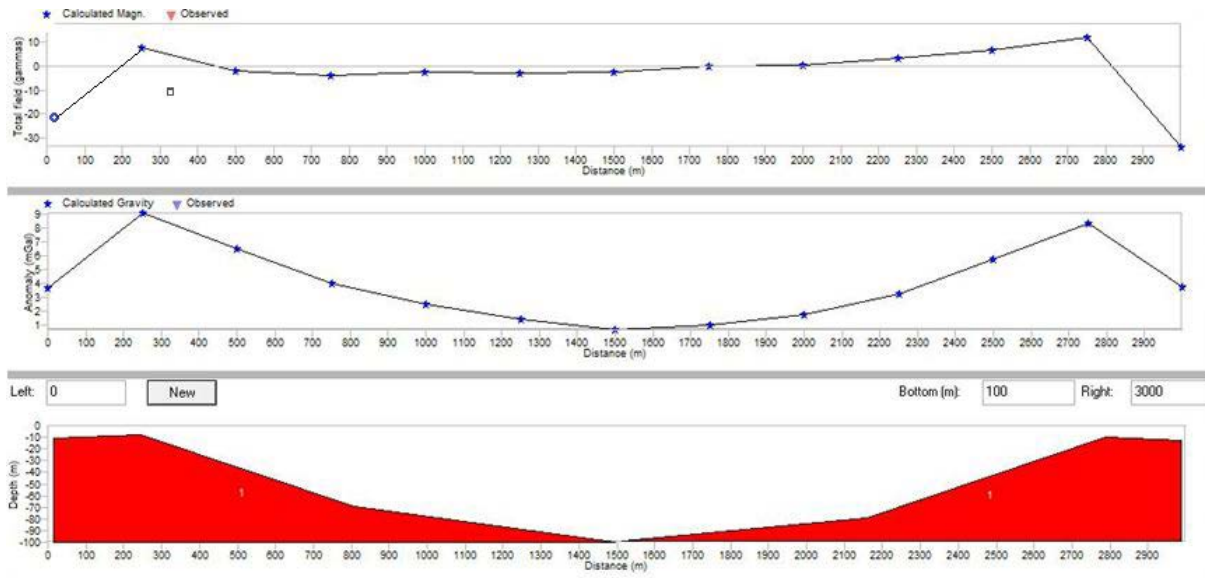


Fig. 6. Geologic cross section and typical magnetic and gravity profile of a hypothetical simple crater.

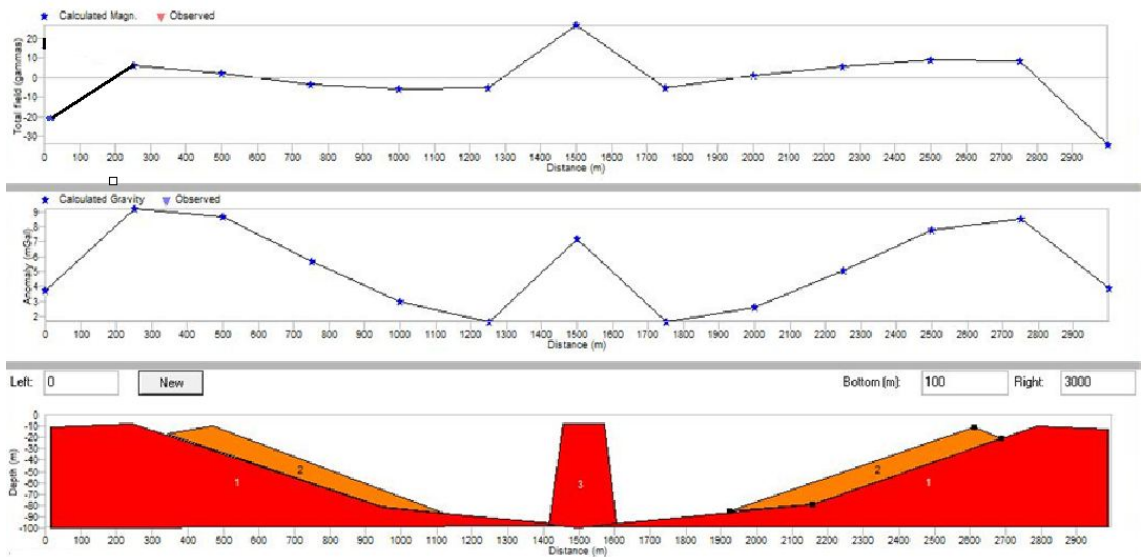


Fig. 7. Geologic cross section and typical magnetic and gravity profile of a hypothetical complex crater.

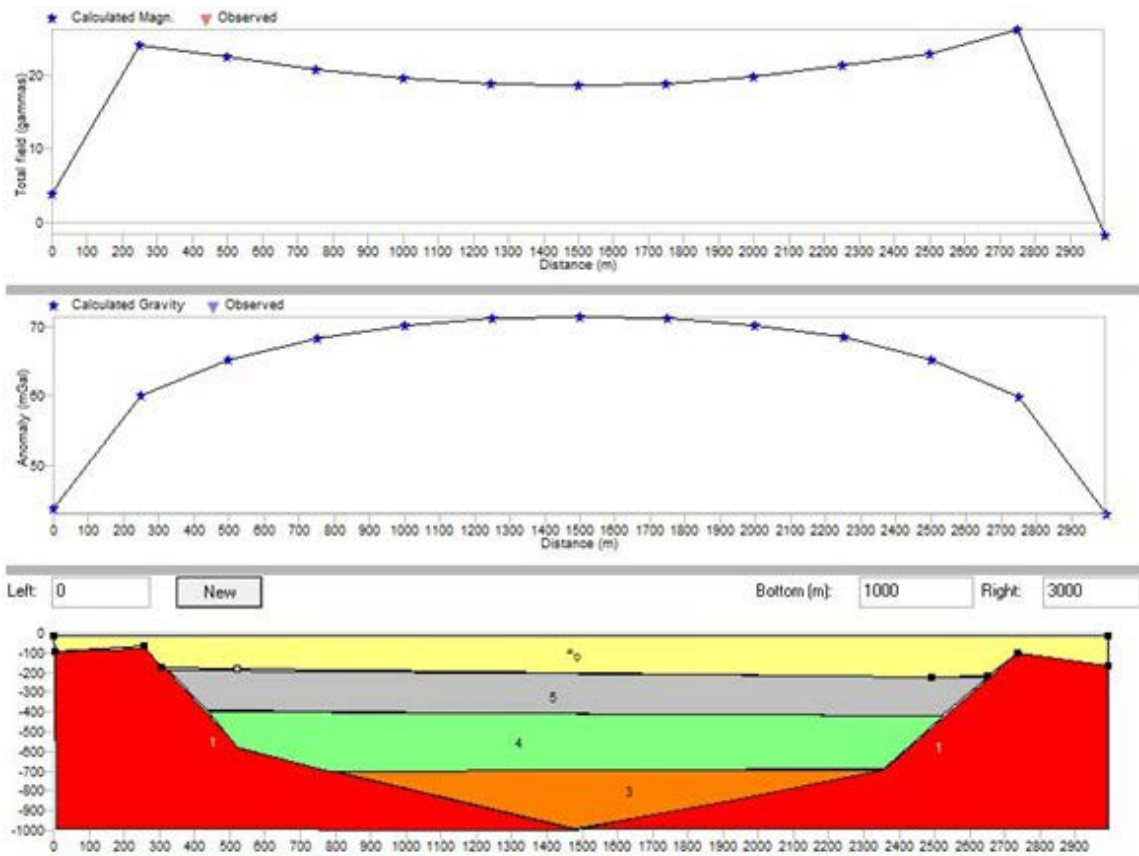


Fig. 8. Geologic cross section and typical magnetic and gravity profile of a hypothetical simple crater with accompanying lithology.

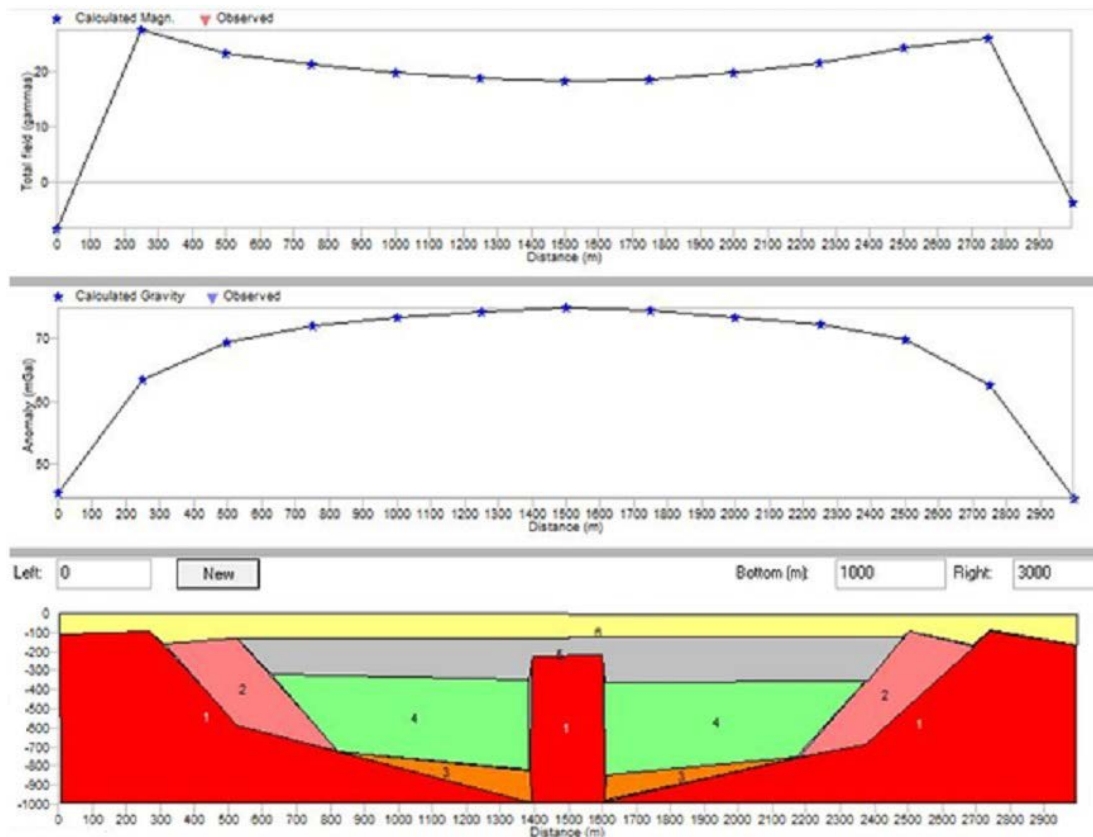


Fig. 9. Geologic cross section and typical magnetic and gravity profile of a hypothetical complex crater with accompanying lithology.

Reflection Seismology

Reflection seismology was first introduced in the early 1920's and by the later part of the decade became more main-stream in the field of seismology. Reflection seismology has some advantages over refraction seismology with one of the primary advantages being short shot-line lengths. However two disadvantages reflection seismology has is the disappearance of low-velocity zones and reflections arrive after other wave making recognition difficult. In the case of this investigation surficial cover consists of a low velocity till and the reflector is high velocity granite.

The primary travel-time equation for reflection profiling is defined as:

$$\text{Time} = (x^2 + 4h_1^2)^{1/2} / V_1$$

and is illustrated by Figure 10, where E is the energy source and G is a receiving geophone. Impact structures are generally only a few kilometers in depth making reflection profiling an ideal method of investigation. A more in-depth discussion of considerations and data processing of reflection seismology are presented in a following chapter.

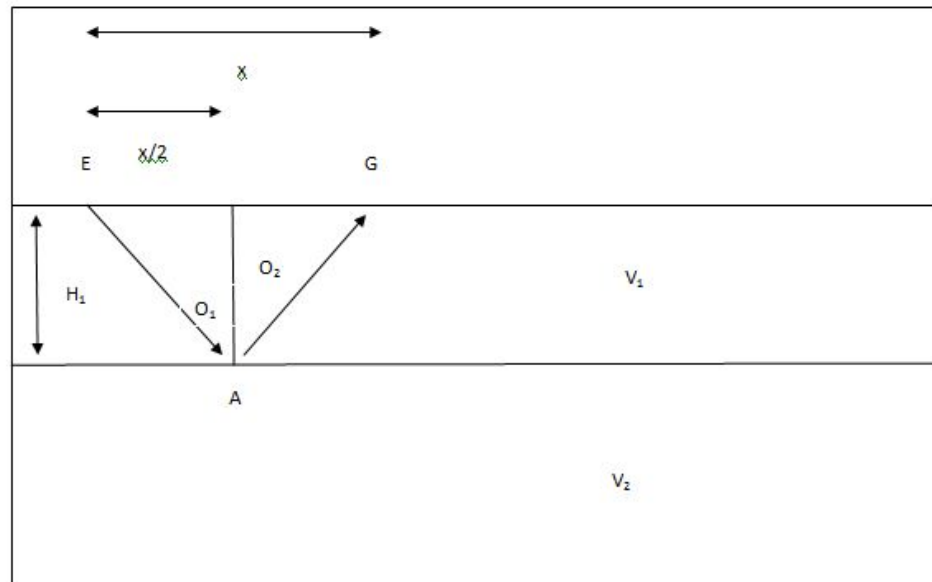


Fig. 10. Diagram indicating symbols used for reflection travel time curves. Modified from Sharma, 1997.

CHAPTER III
PREVIOUS GRAVITY WORK
Gravity Results

Christina Davids (Davids & Gosnold, 1995; Davids, 2002) conducted a gravity survey of the impact structure and surrounding area in 2002. Using data gathered during her survey (Fig. 11) I constructed a Bouguer anomaly map and regional trend maps of the structure. A Bouguer gravity anomaly consists of two components: the regional anomaly and the residual anomaly. The determination of what is considered a regional or residual anomaly is dictated by the scope of the survey.

Large geologic structures generate large wavelength regional anomalies that produce smooth contours over large distances. In this study the Precambrian basement rock and the overlying Interlake Formations are responsible for the regional anomaly and can mask residual anomalies that are of interest. First order, second order, and third order regression regional anomaly maps were produced using Surfer 8™ (Figs. 12-14).

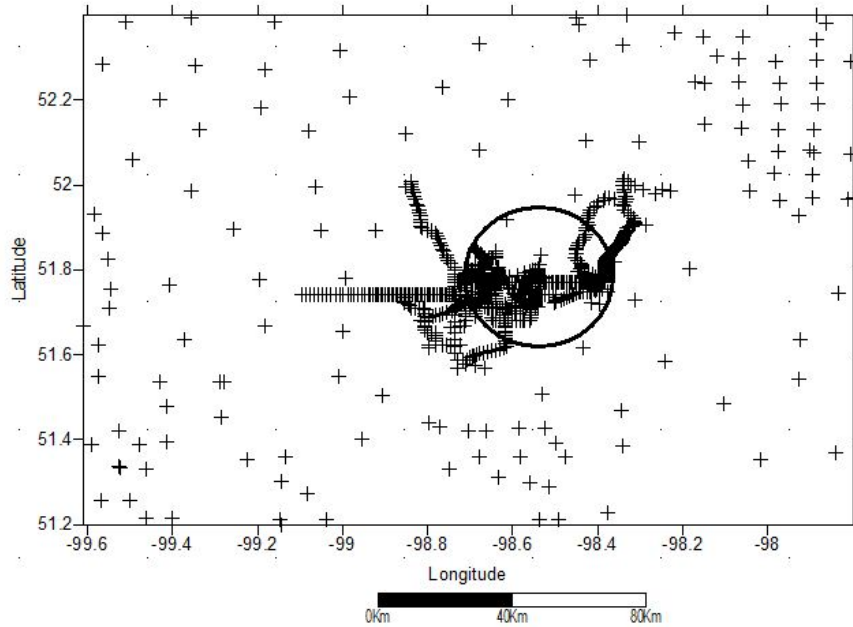


Fig. 11. Gravity survey locations.

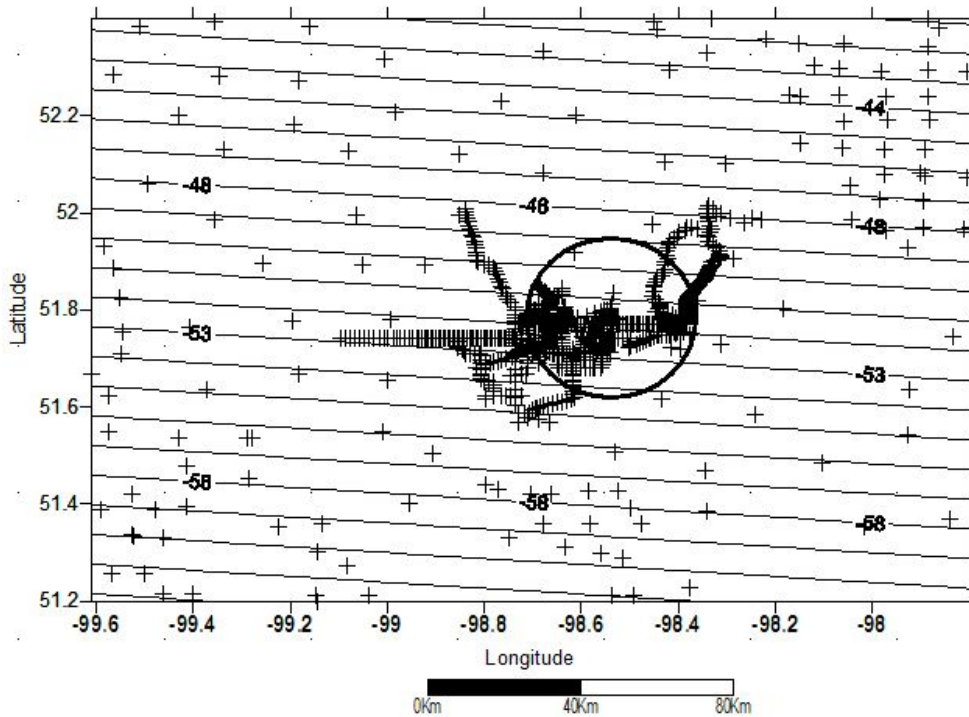


Fig. 12. First order polynomial trend surface of the Bouguer anomaly with the structures outline superimposed.

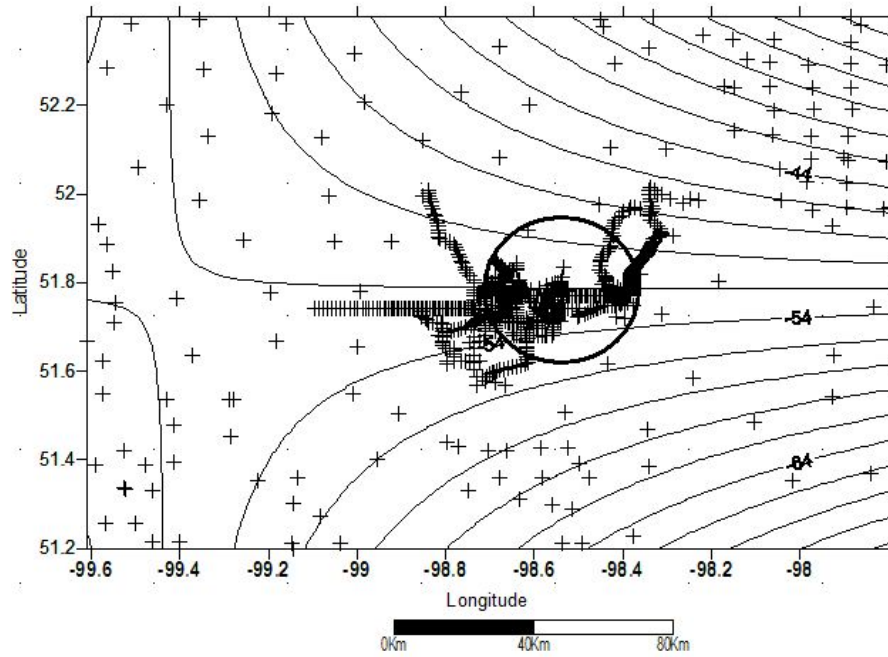


Fig. 13. Second order polynomial trend surface of the Bouguer anomaly.

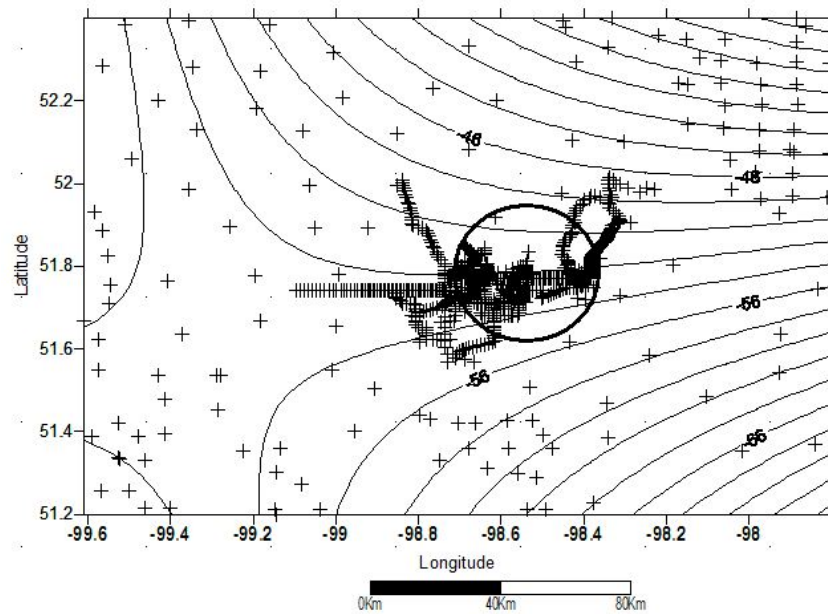


Fig. 14. Third order polynomial trend surface of the Bouguer anomaly.

To produce the Bouguer gravity contour map (Fig. 15) I used the graphical smoothing method in Surfer 8™. The black circle on Fig. 15 delineates the accepted outer limits of the impact structure. At the center of Fig. 15 and moving northeast, contour lines become closely spaced together suggesting that the more dense granite is nearer the surface. This is opposite of what is found southwest where the contour interval is more widely spaced suggesting that the granite is at a deeper depth. A 3D wireframe (Fig. 16) of the Bouguer gravity anomaly illustrates the southwesterly slope of the structure supporting the statement by McCabe and Bannatyne (1970) of post formational tilting of the structure.

Residual anomalies are short wavelength local features such as an ore body, pore space or fracturing within the target rock. In this study possible faults or fractures are the features of interest. First order, second order, and third order residual anomaly maps (Figs. 17-19) were produced by removing the regional anomaly from the Bouguer anomaly map using Oasis Montaj.

Figures 17-19, produced by Dr. Jeffrey Plescia of the Johns Hopkins Applied Physics Laboratory, show that a remnant circular structure associated with the impact event is present after removing the regional field. The differences in gravity values with respect to the impact structure are the result of fracturing within the bedrock, lateral lithologic changes, and depth. The higher the concentration of fracturing present is the less dense the anomaly will appear.

Interpreted in the figures are features associated with a complex crater. The central peak has a diameter of approximately 4 kilometers. Moving laterally away from the central peak the annular trough extends 10 kilometers. Continuing outward from the

annular trough for a distance of 6 kilometers is the structure's rim. An area of disturbed bedrock associated with the impact event but outside the structure's boundary lies past the rim (Pilkington and Grieve, 1992). The data show that Big Rock lies at the accepted boundary distinguishing the structure's maximum extent from the disturbed bedrock outside.

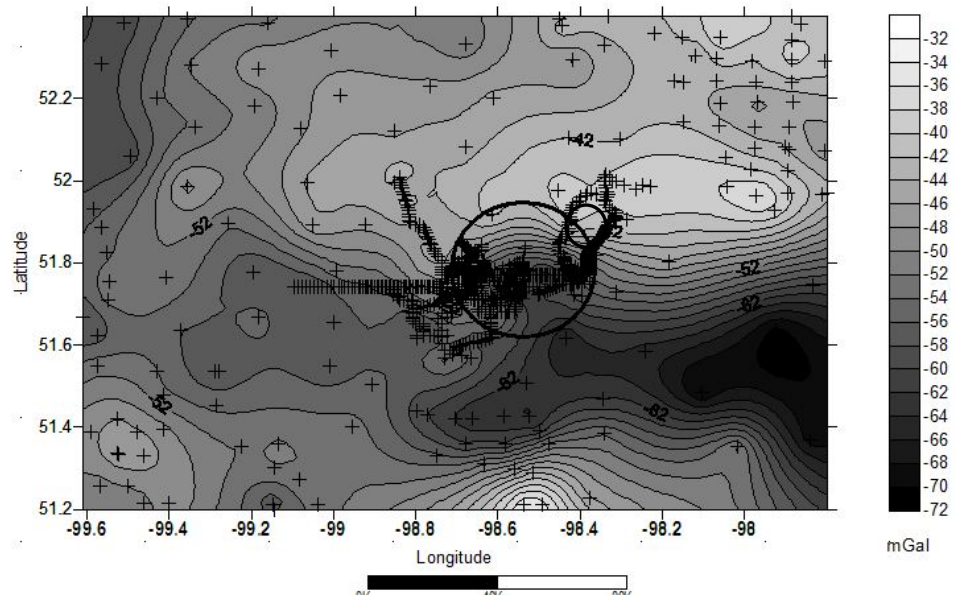


Fig. 15. Lake St. Martin Bouguer gravity anomaly map with gravity station locations.

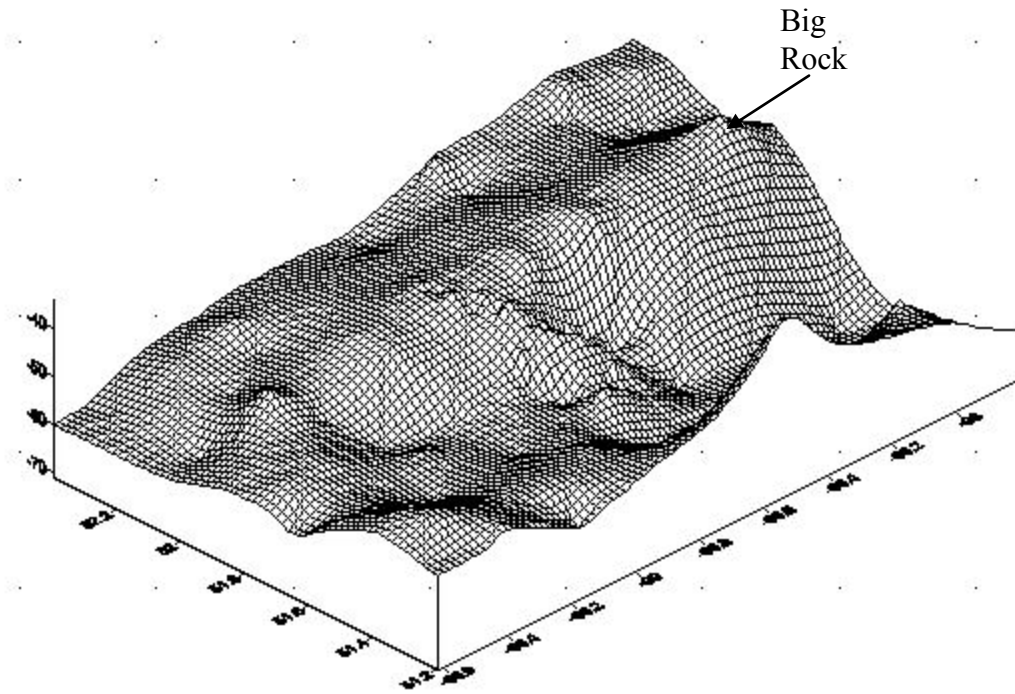


Fig. 16. A 3D wireframe of the Bouguer gravity anomaly map revealing the southwesterly slope of the impact structure.

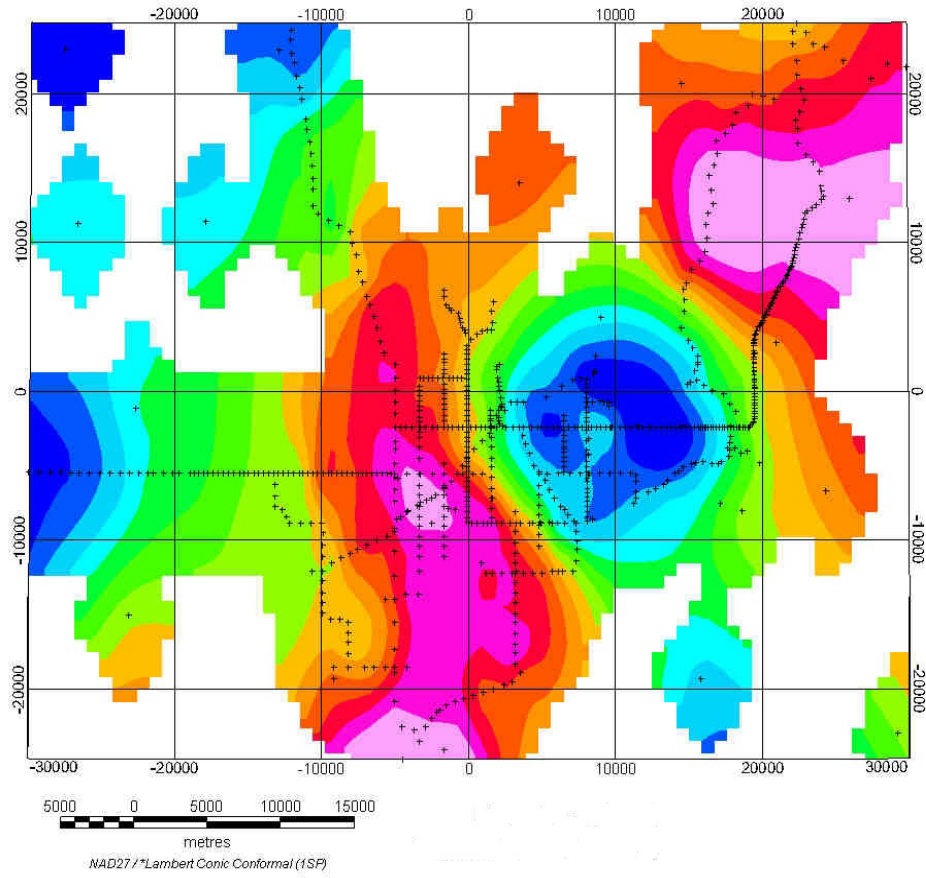


Fig. 17. Lake St. Martin 1st order residual gravity.

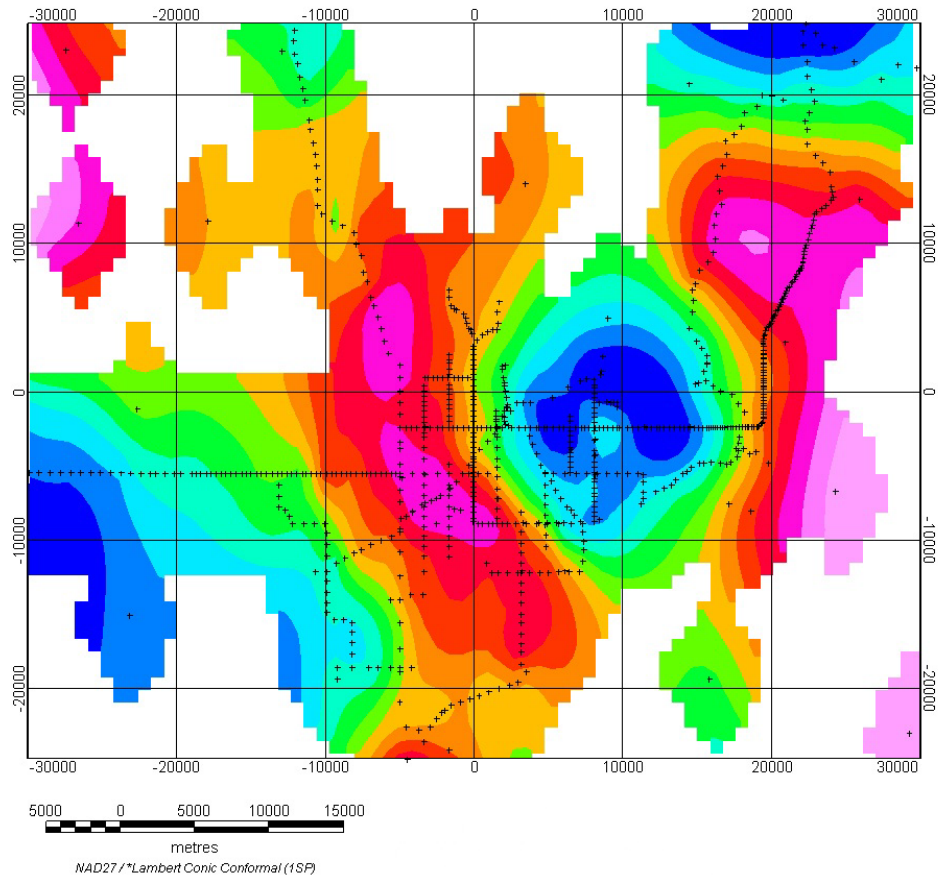


Fig. 18. Lake St. Martin 2nd order residual gravity.

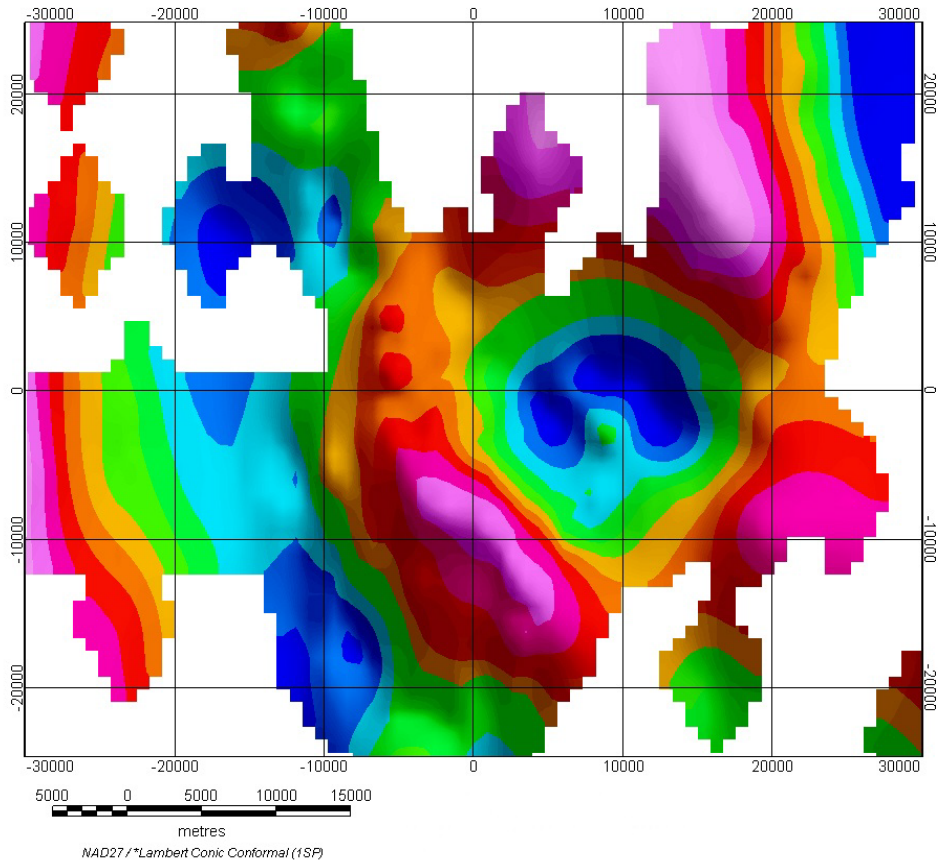


Fig. 19. Lake St. Martin 3rd order residual gravity.

CHAPTER IV

MAGNETICS

Data Acquisition

Magnetic surveys measure either the remnant or induced magnetic field as recorded in rocks. Generally igneous and metamorphic rocks contain minerals that have magnetic susceptibility, such as magnetite or hematite, return a usable signal. The sedimentary rocks in this area do not contain magnetic susceptible minerals and therefore are unsuitable for this type of survey. Magnetic surveys are versatile with one of their applications being subsurface topography mapping. Since Big Rock is composed of Precambrian granite and lies at the structures rim, a magnetic survey is applicable in this study.

The Earth's magnetic field is a vector quantity and is composed of seven vectors. These vectors are: F, the total intensity of the magnetic field, H, the horizontal component, Z, the vertical component, X, the north component, Y, the east component, D, the magnetic declination and I, magnetic inclination.

Magnetic data were acquired (Fig. 20) using a Geometrics G-856AX Memory-Mag Proton Precession Magnetometer during a three-day period in October 2009. The G-856AX has a resolution of 0.1 nT and an accuracy of 1.0 nT. The total magnetic field (F) was measured at one hundred and thirty two-data points at approximately 500 meter intervals along pre-existing roadways, (Table 2).

The equation for the total field is:

$$F = \sqrt{X^2 + Y^2 + Z^2}$$

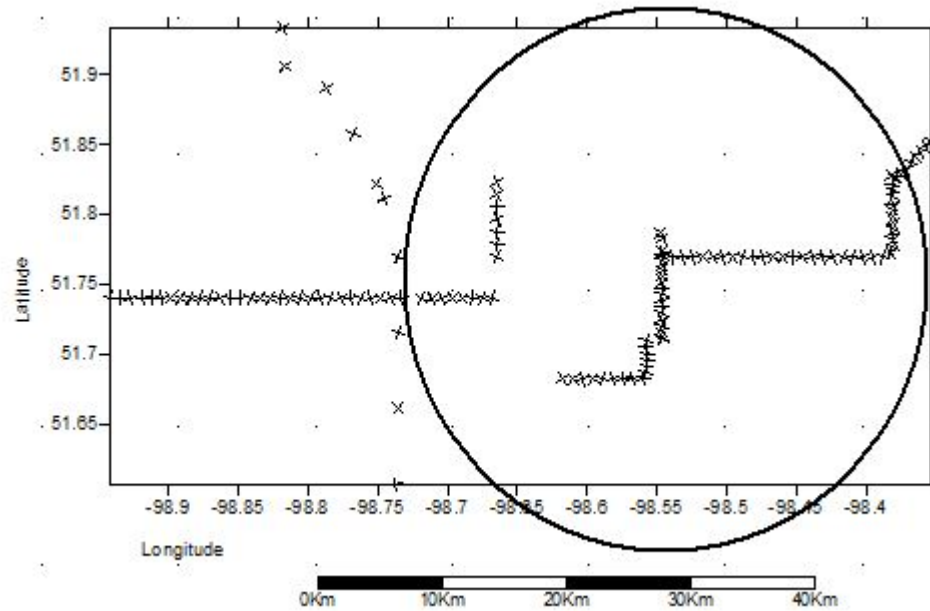


Fig. 20. Magnetic Data Points.

Data Reduction

When reducing magnetic data four corrections need to be considered depending on the type and scope of the survey being conducted. These four corrections are diurnal correction, normal-field correction, elevation, and terrain corrections.

The primary correction to be considered is the diurnal correction. This correction takes into account the temporal variation of the geomagnetic field. The geomagnetic field is a result of particle and electromagnetic radiation from the sun perturbing Earth's ionosphere (Sharma, 1997). Figure 21 represents the daily diurnal variation during the three day magnetic survey. After collecting the magnetic data I entered corrected magnetic values from Table 1 into Surfer 8 and produced a visual representation.

The normal-field correction takes into account the normal variation of the geomagnetic field intensity with respect to latitude and longitude. Due to the size of the survey conducted I did not include this correction. Elevation and terrain corrections take

into account the vertical gradient of the geomagnetic field at the surface of Earth.

Elevation and terrain corrections are not required for this survey since the terrain was flat.

Attenuation of Error

The primary consideration for data integrity in magnetic surveys is what Burger (2006) has called magnetic cleanliness. Burger et. al. (2006) identify some considerations: the removal of all metallic items from the surveyor's person, that the sensor of the magnetometer is at least three meters above the ground, and a distance of at least 20 meters away from vehicles and power lines are maintained. I took care to use these procedures in this investigation to protect the integrity of the data.

Two additional sources of error may affect the data that are beyond user control: the distribution of the mineral responsible for the magnetization and the effect of remnant magnetization. In the first instance, it is possible that an uneven distribution of the source mineral may result in an undesirable signal producing an incorrect interpretation. In the latter instance the measured magnetic anomaly is the combination of induced magnetization and the remnant magnetization, Burger, 2006.

Table 1. Magnetic data point locations with anomaly values

Latitude	Longitude	Reading	Base Station	Diurnal Reading	Latitude	Longitude	Reading	Base Station	Diurnal Reading
51.74033	-98.94158	58763	589500	-530737	51.68241	-98.55978	58376	589637	-531261
51.74032	-98.93460	58761	589759	-530998	51.68692	-98.55821	58456.2	589648	-531192
51.74033	-98.92758	58767	589753	-530986	51.69137	-98.55729	58385.1	589664	-531279
51.74033	-98.91871	58766	589758	-530992	51.69587	-98.55710	58226	589683	-531457
51.74034	-98.91176	58763.8	589760	-530996	51.70032	-98.55725	58235.7	589690	-531454
51.74035	-98.90503	58762	589755	-530993	51.70483	-98.55756	58240.7	589690	-531449
51.74033	-98.89867	58777	589731	-530954	51.70929	-98.55786	58224.3	589690	-531466
51.74032	-98.89188	58765	589707	-530942	51.76945	-98.53911	58272.8	589712	-531439
51.74031	-98.88470	58830	589675	-530845	51.76945	-98.53175	58260.3	589696	-531436
51.74030	-98.87736	58830	589667	-530837	51.76943	-98.52455	58209.3	589738	-531529
51.74031	-98.87018	58823	589655	-530832	51.76945	-98.51728	58352.9	589752	-531399
51.74034	-98.86304	58759	589641	-530882	51.76945	-98.51000	58377.9	589709	-531331
51.74033	-98.85582	58727	589641	-530914	51.76946	-98.50276	58455.3	589709	-531254
51.74035	-98.84865	58728	589632	-530904	51.76946	-98.49555	58439.7	589757	-531317
51.74033	-98.84151	58695	589631	-530936	51.76946	-98.48837	58571.1	589768	-531197
51.74034	-98.83435	58665	589614	-530949	51.76947	-98.48118	58419.9	589771	-531351
51.74032	-98.82715	58607	589642	-531035	51.76948	-98.47395	58513.7	589771	-531257
51.74035	-98.81992	58549	589648	-531099	51.76947	-98.46680	58481	589429	-530948
51.74035	-98.81271	58536	589660	-531124	51.76946	-98.45961	58498.7	589725	-531226
51.74034	-98.80553	58576	589681	-531105	51.76947	-98.45242	58617.6	589709	-531091
51.74035	-98.79836	58584	589701	-531117	51.76946	-98.44516	58537.5	589683	-531146
51.74036	-98.79124	58641	589721	-531080	51.76947	-98.43793	58609.2	589683	-531074
51.74033	-98.78405	58682	589704	-531022	51.76948	-98.43079	58696.5	589683	-530987
51.74034	-98.77679	58776	589750	-530974	51.76945	-98.42357	58705.3	589683	-530978
51.74034	-98.76947	58755	589750	-530995	51.76944	-98.41640	58714.8	589652	-530937
51.74033	-98.76215	58725	589747	-531022	51.76945	-98.40923	58773.8	589609	-530835
51.74033	-98.75498	58658	589639	-530981	51.76944	-98.40211	58821.9	589626	-530804
51.74034	-98.74772	58612	589647	-531035	51.76944	-98.39494	59037	589657	-530620

Table 1. Cont.

Latitude	Longitude	Reading	Base Station	Diurnal Reading	Latitude	Longitude	Reading	Base Station	Diurnal Reading
51.74033	-98.74045	58579	589641	-531062	51.76955	-98.38781	58914.2	589662	-530748
51.74034	-98.73333	58568.8	589651	-531082	51.77220	-98.38223	59956.3	589654	-529698
51.74034	-98.71890	58809.3	589661	-530852	51.77654	-98.38116	58980	589654	-530674
51.74035	-98.71165	58617	589674	-531057	51.78100	-98.38126	58967.2	589654	-530687
51.74035	-98.70436	58793	589674	-530881	51.78550	-98.38130	58930.7	589654	-530723
51.74035	-98.69720	58709.8	589673	-530963	51.79000	-98.38129	58866	589628	-530762
51.74035	-98.68994	58625.4	589679	-531054	51.79444	-98.38126	58827.3	589614	-530787
51.74036	-98.68269	58540	589549	-531009	51.79893	-98.38123	58835.9	589603	-530767
51.74034	-98.67542	58563	589679	-531116	51.80347	-98.38121	58822.1	589591	-530769
51.74036	-98.66814	58550	589657	-531107	51.80800	-98.38120	58777	589582	-530805
51.82762	-98.37756	58806.1	589350	-530544	51.81249	-98.38121	58731.8	589582	-530850
51.82773	-98.38242	58803.2	589491	-530688	51.81698	-98.38122	58743	589582	-530839
51.76954	-98.54642	58488.8	589741	-531252	51.82150	-98.38122	58751.8	589582	-530830
51.77411	-98.54648	58248.9	58941	-692.1	51.82564	-98.37872	58975	589562	-530587
51.77185	-98.54649	58118.6	58941	-822.4	51.82957	-98.37518	59013	589518	-530505
51.78293	-98.54647	57981.9	589749	-531767	51.83343	-98.37170	58867	589575	-530708
51.78709	-98.54767	58048.5	589724	-531676	51.83737	-98.36816	58805	589556	-530751
51.76485	-98.54655	58295.8	589718	-531422	51.84127	-98.36463	58781.1	589552	-530771
51.76051	-98.54653	58310.2	589708	-531398	51.84518	-98.36110	58780	589574	-530794
51.75608	-98.54653	58367	589682	-531315	51.84911	-98.35755	58651	589626	-530975
51.7516	-98.54654	58342.5	589669	-531327	51.85302	-98.35403	58584	589696	-531112
51.74701	-98.54652	58311.8	58969	-657.2	51.82315	-98.66463	58910.1	589610	-530700
51.74251	-98.54652	58376.7	58969	-592.3	51.81464	-98.66457	58920.5	589617	-530697
51.73805	-98.54657	58414	589670	-531256	51.80575	-98.66465	58887.9	589617	-530729
51.73357	-98.54657	58391	589660	-531269	51.79676	-98.66460	58821	589617	-530796
51.72911	-98.54659	58370	589660	-531290	51.78779	-98.66457	58734	589656	-530922
51.72464	-98.54661	58326.9	589660	-531333	51.77881	-98.66458	58792	589709	-530917
51.72017	-98.54659	58450.3	589649	-531199	51.76987	-98.66457	58603	589718	-531115

Table 1. Cont.

Latitude	Longitude	Reading	Base Station	Diurnal Reading	Latitude	Longitude	Reading	Base Station	Diurnal Reading
51.71568	-98.54659	58419	589633	-531214	51.82179	-98.75098	58864.6	589728	-530863
51.71125	-98.54662	58225.4	589612	-531387	51.85763	-98.76770	58513	589719	-531206
51.68211	-98.61732	59267	589605	-530338	51.89025	-98.78726	58794	589761	-530967
51.68214	-98.61015	58425.9	589564	-531138	51.90637	-98.81653	58810	589763	-530953
51.68217	-98.58866	58416.2	589617	-531201	51.76967	-98.73554	58523.7		-58523.7
51.68222	-98.58147	58559.8	589632	-531072	51.71569	-98.73544	58613.3		-58613.3
51.68229	-98.57430	58642.7	589632	-530989	51.66160	-98.73547	58541.1		-58541.1
51.68234	-98.56702	58469.3	589632	-531163	51.60652	-98.73767	58491		-58491
51.68213	-98.60307	58436.7	589602	-531165	51.93356	-98.81867	58742	589800	-531058
51.68214	-98.59589	58385.3	589605	-531220	51.81157	-98.74541	58668	589823	-531155

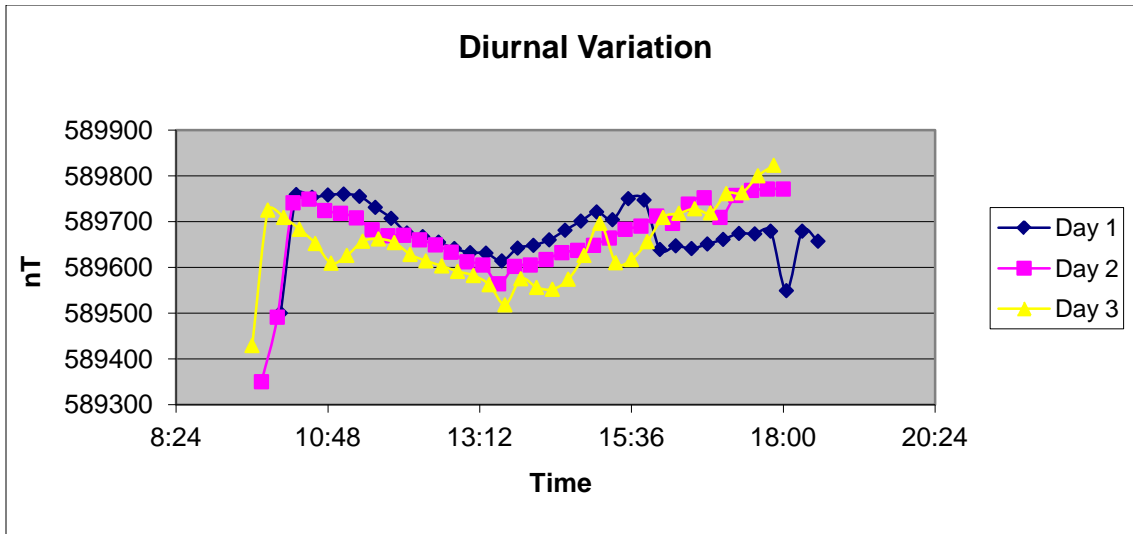


Fig. 21. Daily diurnal variation during the magnetic survey.

CHAPTER V
SEISMIC REFLECTION PROFILING
Data Acquisition

Seismic reflection profiling was conducted along the structures northeast boundary along a 960 meter section of road parallel to Big Rock. The seismic line began at 51.82472/ -98.38057 and ended at 51.83179 / -98.37339, Fig. 22. Three Geometrics Geode exploration seismographs were employed enabling a total of 72 channels to be recorded. The Geode specifications used in this survey are: 24 bit, ultra-high resolution 20 kHz bandwidth (8 to 0.02 ms sampling), low distortion (0.0005%), low noise (0.2uV), stacking accuracy (1/32 of sample interval).



Fig. 22. Ariel view of the location of the seismic reflection line. GoogleEarth, 2010 Terrametrics. Accessed on 12/04/2010.

Energy Source

University of North Dakota students and machine shop employees designed and constructed the source used to generate the necessary energy to conduct the survey. The seismic source, called the BOSS, (Ballistic Ordinance Seismic Source) operates by shooting a 12-gauge shotgun slug into the ground surface, Fig. 23. The impacting slug then produces enough energy to be useful for shallow reflection surveys.



Fig. 23. The Ballistic Ordinance Seismic Source, (BOSS).

Technique

The technique most commonly used for shallow reflection seismic surveys is the common-depth point (CDP) technique, (Fig. 24). The reflector, R in Fig. 24, is the feature that the survey is trying to image. In this method the energy source and receiving

geophones are placed in a linear array. After each completed shot, additional geophones are added to the seismic line and the energy source is advanced linearly along the seismic line after each shot. The CDP technique ensures that the reflection point, R, is common to all points on the seismic line. A field laptop computer records the shot data for later retrieval and reduction.

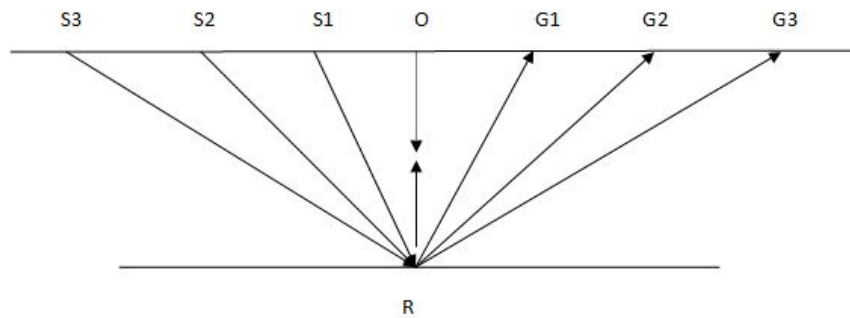


Fig. 24. Ray paths of reflections belonging to the common depth point (CDP) which is located below the shot-geophone common midpoint, O. Modified from Sharma, 1997.

Normal Move Out

Normal move out is the difference in reflection times from a horizontal reflecting surface due to variations in the source-geophone distance. In reflection surveys normal move out (NMO) is the principle criterion to identifying if the event observed is a reflection (Sharma, 1997) and assists in determining the proper geophone spacing.

Data Reduction

The seismic reflection data obtained during the survey were then reduced using the outside seismic data processing consultant Divestco. This was necessary due to the complexity associated with seismic reflection data processing. Keiswetter, Black and Steples (1996) provide a typical data processing flow chart in Table 2. The objective of

seismic data reduction is to incorporate multiple shot points obtained during a survey into one coherent subsurface profile, Fig.25

Table 2. Data Processing Flow

Convert raw data into processing format
Apply geometry formation
Remove bad/noisy traces
Automatic Gain Control (AGC) scale
Frequency-wave number (FK) filter
Frequency filter (time variable)
Dip-moveout corrections
First arrival mute
Air-wave mute
Ground-roll mute
Elevation corrections
Sort into CDPs
Velocity analysis
CDP Stack
Post-stack bandpass filter
Trace equalization
Display

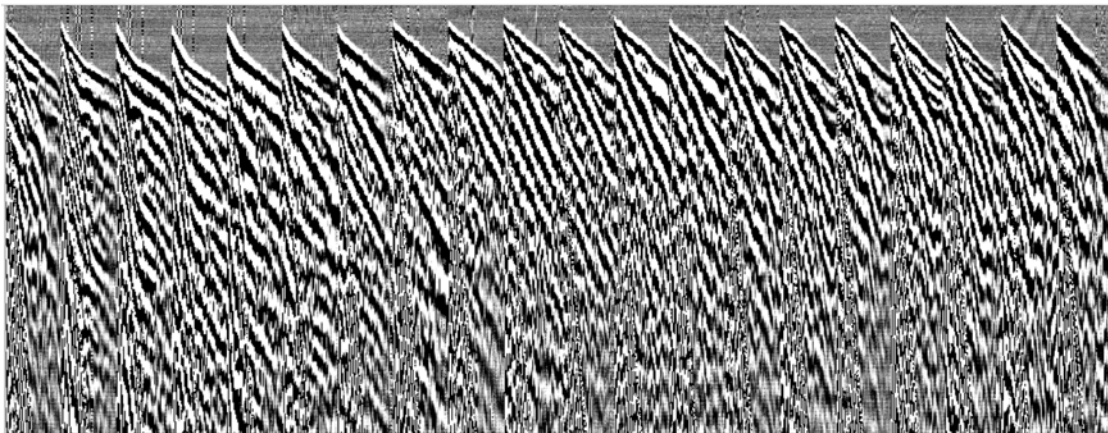


Fig. 25. Multiple seismic shotpoints from the seismic line prior to data processing.

CHAPTER VI

RESULTS

Gravity

Dauids' gravity study contained 699 gravity stations of which I have selected thirteen data points. Gravity points I selected profile the seismic reflection and magnetic profiles I produced of Big Rock and are presented later in this manuscript. The gravity profile (Fig. 26) began 560 meters to the front of the seismic line and ended 368 meters beyond the seismic line for a total length of 1.9 kilometers. Gravity station identification numbers 5 through 11 are the approximate boundaries of the seismic line.

Selected gravity data from Dauids' thesis (2002) are presented in Table 3.

Observed gravity is the gravity value recorded at a specific location. Theoretical values are predicted gravity values on a reference ellipsoid at sea level based on latitude.

Observed gravity and theoretical values are recorded in mGals. The following equation, as accepted by the International Union of Geodesy and Geophysics (IUGG) as the basis for the Geodetic Reference System in 1967 (GRS 1967), is used to calculate the normal gravity at latitude ϕ and takes into account the flattening effect of the ellipsoid and rotation of Earth:

$$g_{\phi} = 9.780319(1 + 0.0053042 \sin^2 \phi - 0.0000059 \sin^2 2\phi) \text{ m/s}^2$$

Table 3. Selected gravity stations used in the gravity profile of Big Rock. From Davids, 2002

Station ID	Latitude	Longitude	Elevation	Observed	Free Air	Bouguer
LSM124	51.819	-98.382	249.7	981131.49	-22.19	-50.13
LSM125	51.82	-98.382	249.7	981131.92	-21.85	-49.79
LSM126	51.821	-98.382	249.7	981132.82	-21.04	-48.97
402078	51.822	-98.381165	248.1	981132.8	NR	-49.42
LSM127	51.824	-98.381	249.8	981133.41	-20.68	-48.63
LSM128	51.825	-98.38	249.8	981133.69	-20.49	-48.44
LSM129	51.827	-98.379	249.7	981134.16	-20.23	-48.16
LSM130	51.829	-98.378	249.4	981134.96	-19.7	-47.6
LSM131	51.83	-98.376	248.9	981135.43	-19.47	-47.32
LSM132	51.831	-98.375	248.4	981135.69	-19.45	-47.24
LSM133	51.832	-98.374	247.9	981135.97	-19.41	-47.15
LSM134	51.833	-98.373	247.7	981136.22	-19.31	-47.02
LSM135	51.835	-98.372	247.5	981136.41	-19.36	-47.05

Gravity investigation results reveal that between the sampled gravity stations a shallowing of basement rock occurs with exposure at Big Rock (Fig. 26). Additionally an anomalous feature was indicated that may be interpreted a fracture or fault in the profile. This interpreted feature lays between gravity stations three and five which shows a sudden decrease in the gravity value. The association of a decrease in the gravity value to a fracture or fault interpretation is that fracturing reduces the density of the underlying lithology, which then reduces the gravity value. In this interpretation gravity station eleven is considered the outer boundary of the impact structure.

Depth to the feature at gravity station three was estimated by determining where the total change in gravity (Δg_{max}) falls to its half value. The horizontal distance, x_f , over which the anomaly changes from $0.5 \Delta g_{max}$ to $0.25 \Delta g_{max}$ is a measure of the depth, (Sharma, 1997). At gravity station four, the depth to the anomaly was determined to be 28 meters. Gravity stations eleven and beyond are determined to be near the surface.

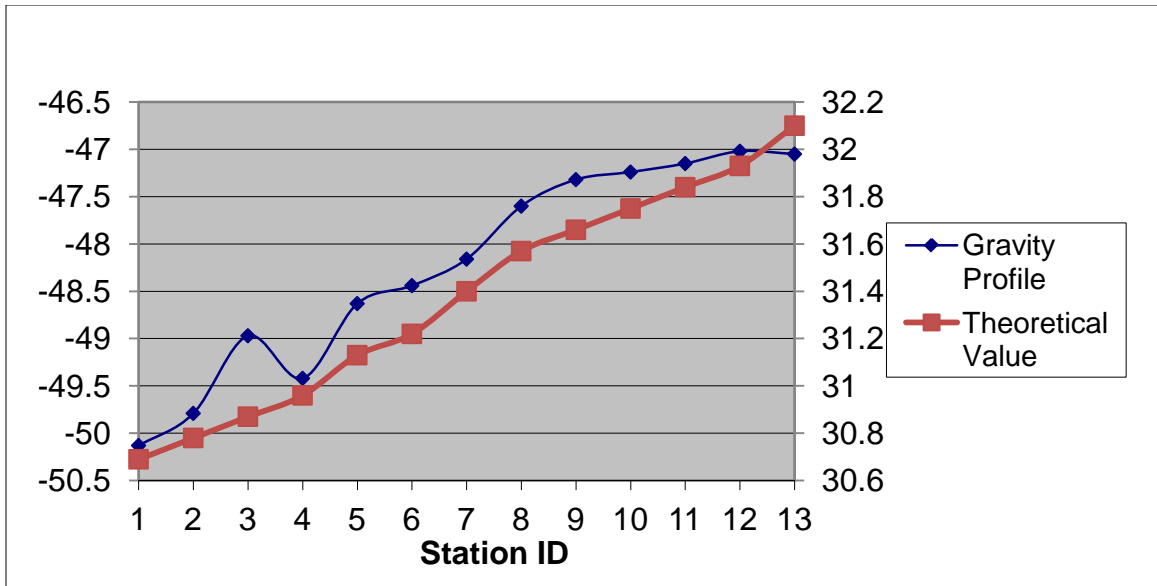


Fig. 26. Observed gravity profile with theoretical values.

Magnetic

I reduced magnetic survey data to produce a magnetic anomaly map of the impact structure using the program Surfer 8, Fig. 27. The crosses show magnetic reading locations. A large black circle outlines the approximate structure boundary. The small black circle shows the location of Big Rock. Identified towards the center of the impact structure is the central peak. Individual features are not well identifiable at this scale however the structures southwest tilt is observed as indicated by the decrease in anomaly value.

A three kilometer, six point magnetic profile of the total field anomaly was produced to include the seismic line, Fig. 28. The seismic line consists of points three, four, and five for a total length of approximately one kilometer. Results of the magnetic profile show that the bedrock is shallowing. The parabola that is between points two and five on Fig. 28 may suggest a high angle fault or fracture.

Depth to the top of the magnetic anomaly was determined by the 'slope' (d) method (Peters, 1949). The slope method: $z = d/1.6$, where Peters (1949) define d as the horizontal interval where the steepest part of the anomaly curve is essentially a straight line. Using this method on the left side of the slope suggests a depth of 103 meters and on the right side of the slope a depth of 102 meters. This result suggests that there is a shallowing of the basement rock. Additionally, between magnetic stations two through five (Fig. 28) a parabola is present that may be interpreted as a high angle fault or fracture.

Figure 29 illustrates a corroborating geologic profile based on the selected magnetic and gravity data along the seismic reflection line and was produced using the commercially available software GravMag. Included in the figure are the theoretical and observed values for both the gravity and magnetic data values. Parameters selected for the magnetic profile include: remnant magnetics, a 30° azimuth, and 51.81° latitude. A density of 2.67 g/cm³ for the granitic basement rock (red unit) and 2.0 g/cm³ for the surficial cover (yellow unit) were used for the gravity profile.

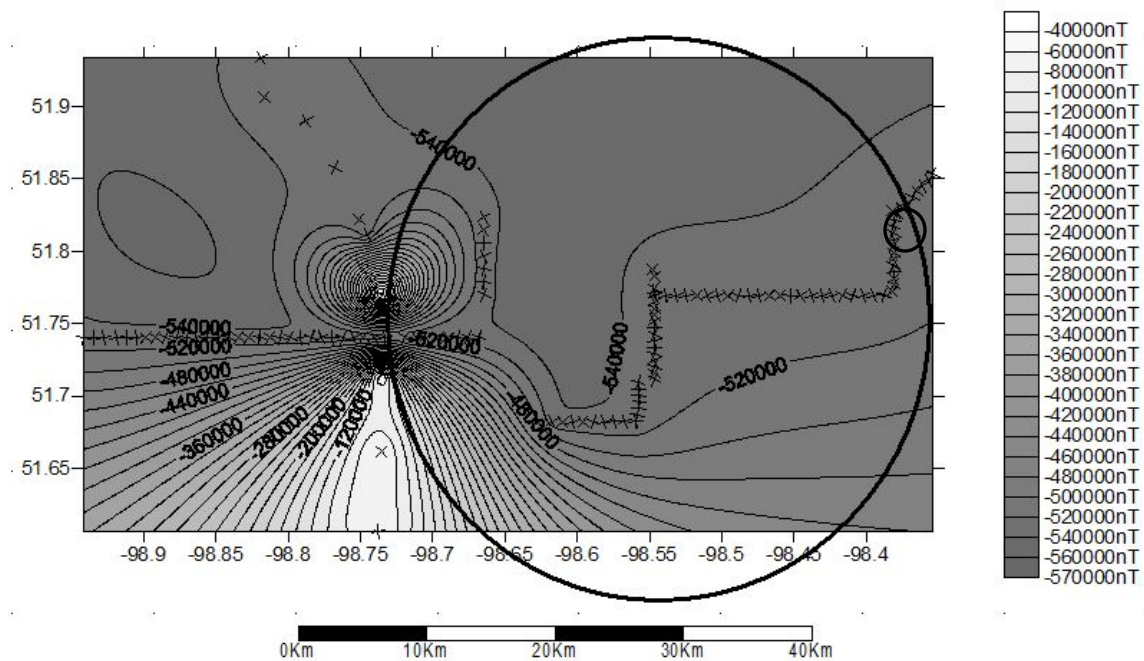


Figure 27. Remnant magnetic field strength and data points with superimposed crater boundary.

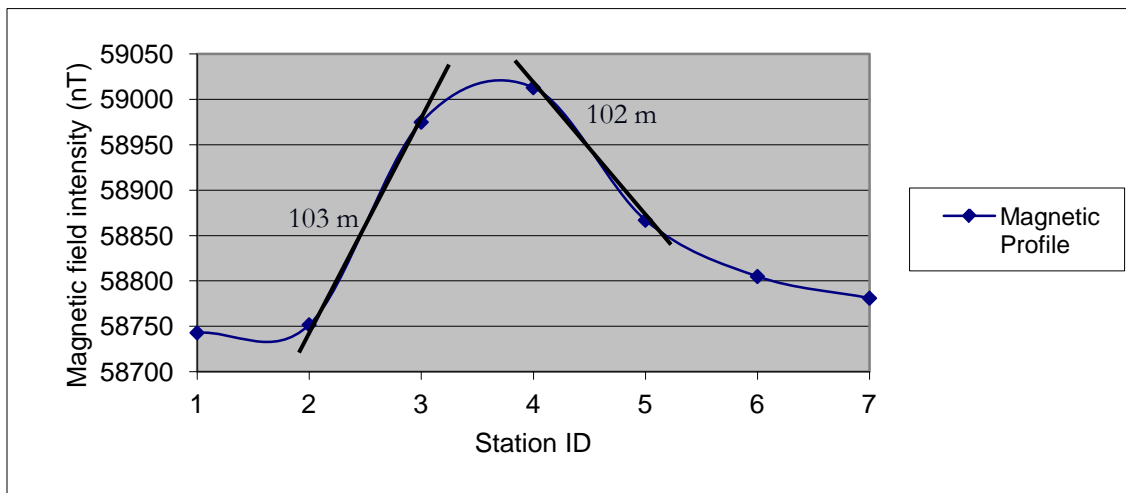


Fig. 28. Magnetic profile of seismic line with depth to anomaly.

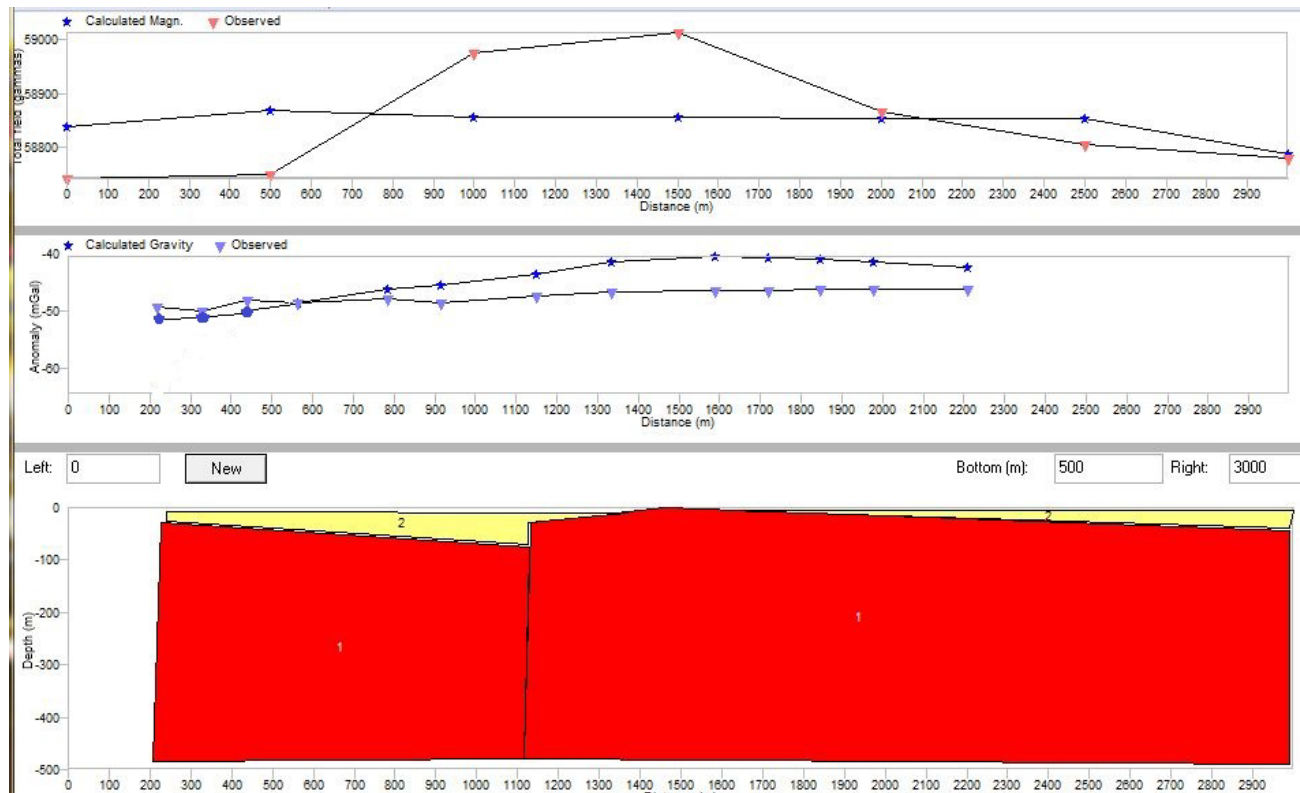


Fig. 29. Combined geologic profile with accompanying gravity and magnetic data.

Seismic Reflection Profiling

The results of the seismic reflection survey were a partial success with the success being that the survey was able to image the granitic basement rock near the surface. The seismic reflection survey does reveal a shallowing of the basement rock with exposure near Big Rock, which then becomes buried again, Fig. 30. Horizontal exaggeration on Fig. 30 is 15x. Not identified, that I was hoping to corroborate, was a possible listric fault that appears on a historical cross-section. This cross section produced by Reimold et. al, (1990) depicts a listric fault that was based on previous drilling activity in the vicinity of Big Rock. There are two primary factors as to why this fault might not have been imaged: first, our seismic line was not long enough to intersect the fault, and second, the fault does not exist.

The lithology along the seismic line include both till and granite. Typical velocities of the primary waves of till range from 1500 ms^{-1} to 2600 ms^{-1} , metamorphic rock velocities range from 3500 ms^{-1} to 7000 ms^{-1} , and granite and gneisses velocities range from 5000 ms^{-1} to 6200 ms^{-1} . Since the seismic velocities of various lithologies may significantly overlap due to factors such as saturation, compaction or fracturing there is not always a unique solution (Burger, et. al., 2006).

The depth to the basement rock varied throughout the seismic line. Depth and velocities were determined using the $x^2 - t^2$ method, Fig. 31. Depth to bedrock at the beginning of the seismic line is 23 meters and has a velocity of 2376.91 ms^{-1} , Fig 32. The midpoint has a depth of 19 meters and a velocity of 3641.79 ms^{-1} , Fig. 33. At the last point bedrock is at a depth of 21 meters and a velocity of 2845.55 ms^{-1} , Fig. 34.

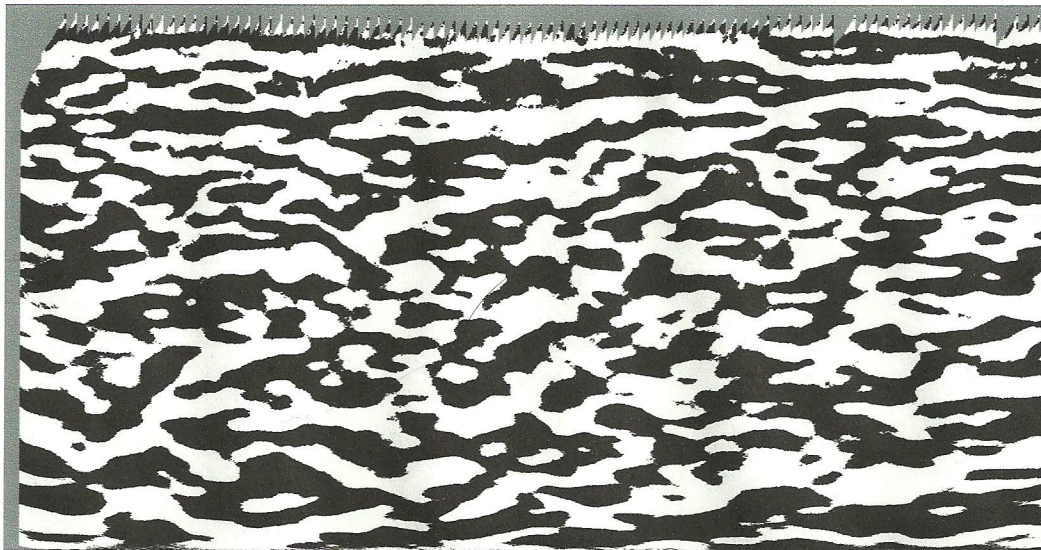


Fig. 30. Seismic reflection image of Big Rock depicting associated features.

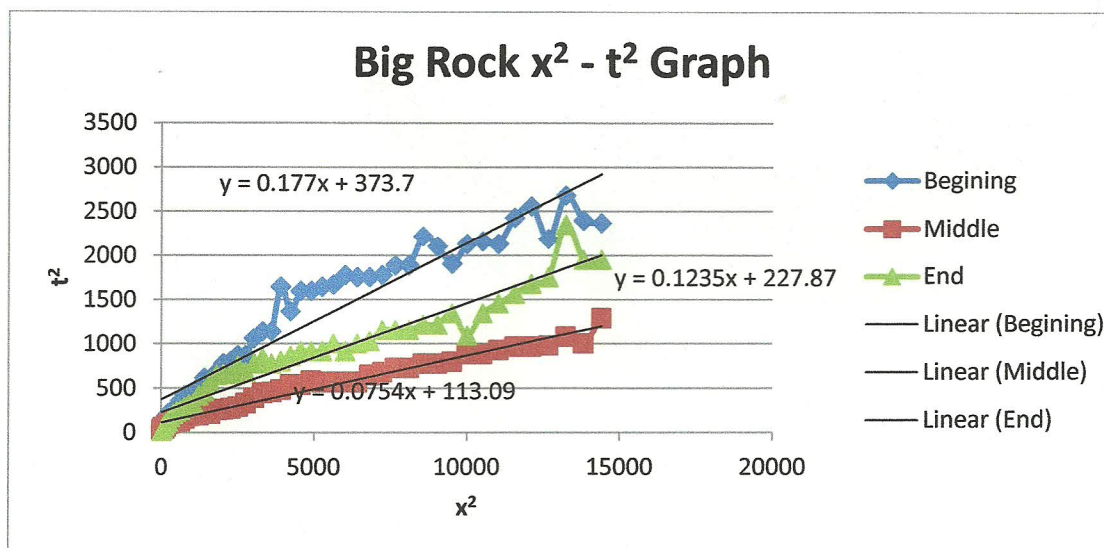


Fig. 31. $x^2 - t^2$ values of three shot locations used to determine velocity and thickness.

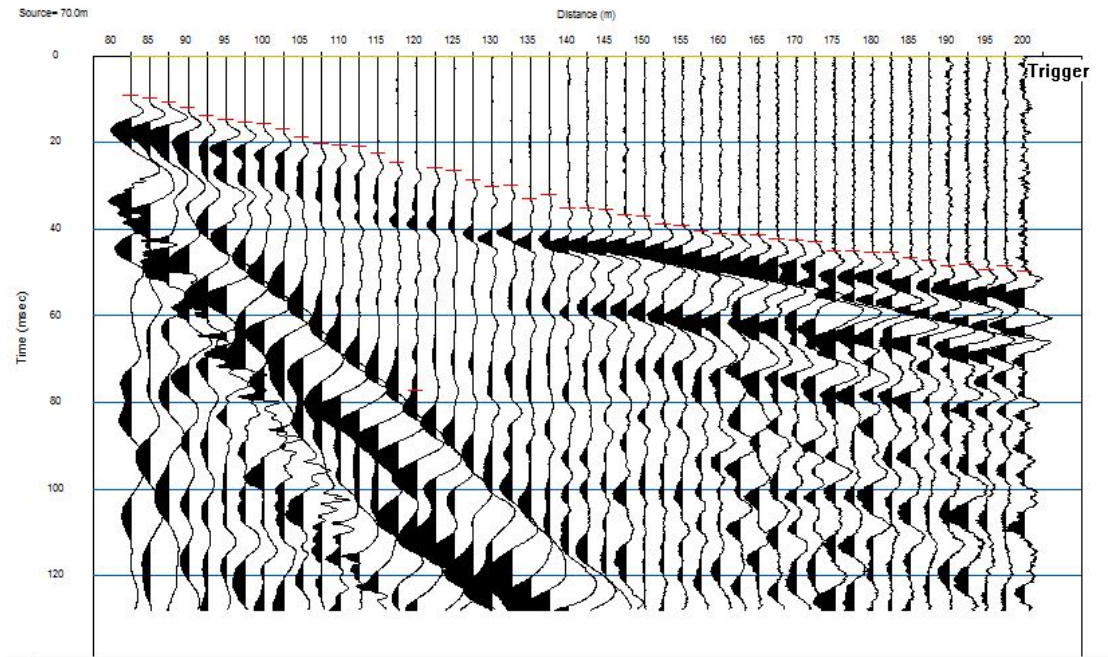


Fig. 32. Beginning shot gather with first breaks.

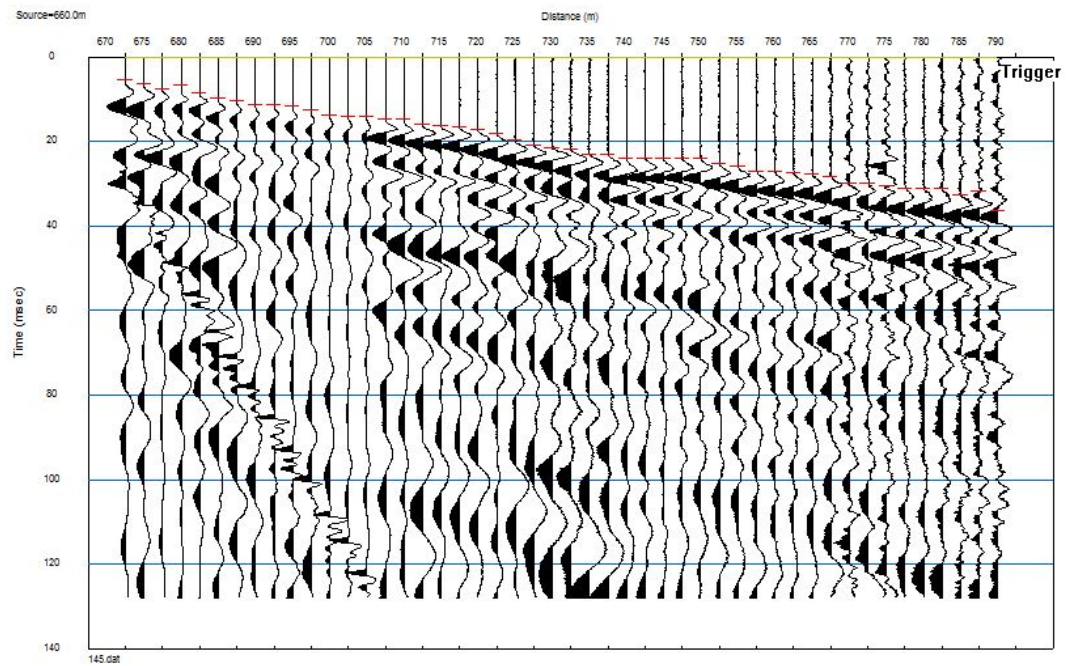


Fig. 33. Middle shot gather with first breaks.

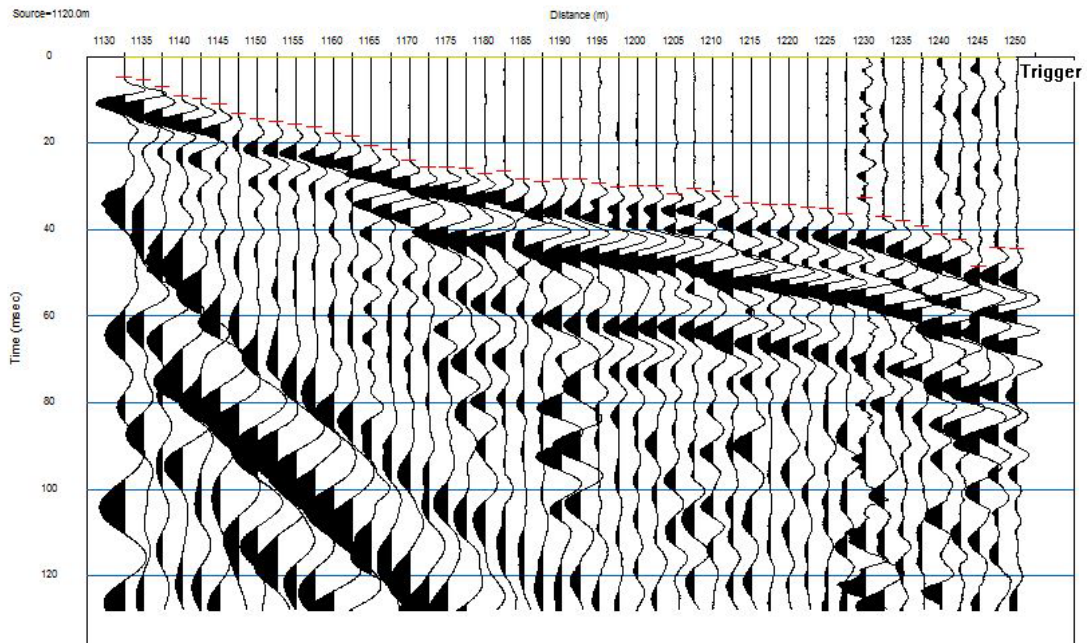


Fig. 34. Last shot gather with first breaks.

CHAPTER VII

DISCUSSION

Large impact events are violent occurrences that release pressure in the GPa range and produce features associated with a resultant crater. The St. Martin impact structure is a complex crater consisting of a central peak, annular trough and rim. Wartho (2009) has re-evaluated the age of the structure using the (U-Th)/He technique and determined it to be between 224.3 Ma and 241.4 Ma. This revised age nullifies a previous hypothesis that the St. Martin impact event occurred as a part of a multiple impact event approximately 213 Ma (Spray, et. al., 1998).

Each geophysical method used in this study has its limitations. The magnetic and gravity methods' limitations are similar in that there is a lack of resolution in subsurface detail. Examples of subsurface detail resolution limitations are multiple faults or fractures found close to one another, fine alternating sedimentary layers, or even the difference between igneous and metamorphic rocks. With respect to seismic reflection profiling the primary limitations to consider are the reflections from subsurface density contrasts. Density contrast reflections arrive at geophones at almost the same time as the higher amplitude ground roll and air blast making them difficult to image. Reflections from greater depths arrive at geophones after the ground roll and the air blast has passed, making deeper targets easier to profile.

Both the gravity anomaly profile and magnetic anomaly profile reveal that there is a shallowing of the basement rock. Additionally along both profiles in the identical location an anomalous feature is observed that still may be attributed to a listric fault. Unfortunately the seismic reflection profiling did not reveal and corroborate the presence of a fault.

The lack of any significant exposed structure is the direct result of post formational tilting. This post formational tilting dips about 0.95 meters per kilometer towards the southwest. This tilting in conjunction with modern day erosion has resulted in the exposure of Big Rock and accounts for the lack of crater rim exposed at the southwestern boundary of the structure, (McCabe, H. R., and Bannatyne, R. B., 1970).

According to the Earth Impact Database, 178 impact structures on Earth are recognized. This number continues to increase each year with the discovery of three to five new impacts (Grieve and Pesonen, 1992). This quantity is not as high on Earth as expected when compared with what can be readily counted on the Lunar or Martian surfaces. Visible extraterrestrial craters are rare because Earth is a dynamic planet with an atmosphere that constantly erodes higher elevations to base level and plate tectonics that recycle the planet's surface. The present day St. Martin impact structure, with its lack of surface expression, is an example of how these erosional processes erase surface features. With no evident surface features, the St. Martin structure has been almost completely characterized completely by geophysical methods.

REFERENCES CITED

- Bannatyne, R.B. 1959, Gypsum-Anhydrite Deposits of Manitoba, Manitoba Mines Branch Publication 58-2, 46p.
- Burger, H. R., Sheehan, A. F., et. al., 2006, Introduction to Applied Geophysics: Exploring the Shallow Subsurface, Norton & Company, p. 554.
- Davids, C. and Gosnold, W. D., 1995, Gravity survey of the Lake Saint Martin impact structure, southern Manitoba, Abstracts with Programs - Geological Society of America, Vol. 27, Issue 6, pp. 208.
- Davids, C., 2002, A high resolution gravity survey of the Lake St. Martin impact structure, Manitoba, Canada, M.S. University of North Dakota, 155 p.
- Earth Impact Database, 2011, <http://www.passc.net/EarthImpactDatabase/index.html> (Accessed: 1/26/2011)
- Grieve, R. A.F. and Pesonen, L. J., 1992, The Terrestrial Impact Cratering Record, Tectonophysics, 216, p. 1-30.
- Keiswetter, D., Black, R., Steeples, D., 1996, Structure of the terrace terrane, Manson impact structure, Iowa, interpreted from high-resolution, seismic reflection data, Geol. Soc. Amer., Special Paper 302, 105 p.
- Kohn, B. P., Osadetz, K. G., and Bezys, R. K., 1995, Apatite fission-track dating of two crater structures in the Canadian Williston Basin, Bull. Can. Petroleum Geology, V. 43, p. 54-64.
- Melosh H. J. 1989. Impact cratering: A geologic process. New York: Oxford University Press, p. 245.
- McCabe, H. R., and Bannatyne, R. B., 1970, Lake St. Martin crypto-explosion crater and geology of the surrounding area, Geol. Paper, 3/70, 79 pp., Manitoba Mines Branch, Dept. of Mines And Natural Resources, Winnipeg, Canada.
- Parasnis, D. S., 1997, Principals of Applied Geophysics, Chapman & Hall, 431p.
- Peters, Leo J., 1949, A direct approach to magnetic interpretation and its practical application, Geophysics, V. 14, p. 290-320.
- Pilkington, M. and Grieve, R. A. F., 1992, The geophysical signature of terrestrial impact craters, Rev. of Geophys, v. 30, p. 161-181.

Reimold, W. U., Barr, J. M., Grieve, R. A. F., & Durrheim, 1990, Geochemistry of the Melt and Country Rocks of the Lake St. Martin Impact Structure, Manitoba, Canada, *Geochimica et Cosmochimica Acta*, v. 54, p. 2093-2111.

Sharma, P., 1997, *Environmental and Engineering Geophysics*, Cambridge University Press, 475p.

Spray, J. G., Kelley, S. P., and Rowley, D. B., 1998, Evidence for a late Triassic multiple impact event on Earth, *Nature*, v. 391, p. 171-173.

Steenland, N. C., 1965, Oil Fields and Aeromagnetic Anomalies, *Geophysics* v. 30, p. 706-739.

Stott, Donald F., 1955, *Jurassic Stratigraphy of Manitoba*, Manitoba Department of Mines and Natural Resources, Mines Branch Pub. 54-2

Wartho, J-A, Schmieder, M, et. al, 2009, New (U-Th)/He zircon and apatite ages for the Lake Saint Martin Impact Structure (Manitoba, Canada) and implications for the Late Triassic multiple impact theory, In: *Abstracts of Papers Submitted to the Lunar and Planetary Science Conference, 2009, Vol. 40.*